FFRS: A computer program for the thermal and mechanical analysis of fuel rods

Misfeldt, I.

Publication date:
1978

Document Version
Publisher's PDF, also known as Version of record

Risø Report No. 373

Risø Report No. 373

Risø National Laboratory

FFRS: A Computer Program for the Thermal and Mechanical Analysis of Fuel Rods

by Ib Misfeldt

February 1978

Sales distributors: Jul. Gjellerup, Sølvgade 87, DK-1307 Copenhagen K, Denmark

Available on exchange from: Risø Library, Risø National Laboratory, P.O. Box 49, DK-4000 Roskilde, Denmark

INIS Descriptors

F CODES
FUEL PELLETS
FUEL RODS
FUEL-CLADDING INTERACTIONS
MECHANICAL PROPERTIES
PERFORMANCE
SIMULATION
URANIUM DIOXIDE
WATER COOLED REACTORS
WATER MODERATED REACTORS
ZIRCALOY

UDC 621.039.548 : 681.3.06 : 519.283

Risø Report No. 373

FFRS: A COMPUTER PROGRAM FOR THE THERMAL AND MECHANICAL ANALYSIS OF FUEL RODS

Ib Misfeldt

Department of Reactor Technology

Risø National Laboratory
February 1978

ABSTRACT

FFRS, a computer code for simulation of in-pile fuel rod performance, was developed for use in reliability predictions for LWR fuel.

As this application involves numerous fuel simulations, the model is sufficiently simple to allow for fast computer calculation, but still detailed enough for realistic simulations.

Detailed descriptions of the stationary thermal and mechanical models are given together with the methods of solution for time-dependent irradiation conditions. Models describing the important material properties for zircaloy, UO_2, and the gap between fuel and cladding are included in the code.

The influence of various parameters in the model has been investigated.

The performance of FFRS was examined through the simulation of a large number of irradiation experiments, including sensitivity studies for some of the material properties.

It is demonstrated that FFRS can very accurately model average fuel behaviour under normal operational conditions with very low computer costs.

This report is submitted to the Technical University of Denmark, in partial fulfilment of the requirements for obtaining the lic. tech. (Ph.D.) degree.

ISBN 87-550-0510-1

CONTENTS

Page

1. INTRODUCTION

Though the general performance of LWRs has been considerably improved during recent years, problems with failures caused by pellet-cladding interaction (PCI) still exist. The occurrence of PCI failures indicates a statistical problem, because they occur at power values far below the threshold values for failures found in irradiation experiments, or calculated by deterministic fuel models. Therefore it was found reasonable to start a project on the statistical evaluation of the failure probability (or the reliability) of fuel rods.

A fast fuel model was needed, as a tool for the statistical evaluation of the fuel reliability, as the statistical methods considered require a large number of simulations in each case. The model needed to be orders of magnitude faster (in computer time) than the existing Danish fuel performance code WAFER[1], but not necessarily self-contained, as it could be adjusted by comparison with WAFER. Correct response to reasonable changes in the design data, material properties and operational conditions was the desired capability of the model. As PCI failure was the type of failure considered most important, modelling was concentrated on fuel-cladding contact situations.

The approach chosen was very successful compared to other fuel models, therefore the model was completed as a self-contained fuel performance code, FFRS*). After completion of the code, it was tested on several sample problems. The results are generally in as good agreement with experimental work as are the predictions made by state-of-the-art fuel models; the fuel-cladding contact results seem especially successful.

2. THE STATIONARY FUEL ROD MODEL

A slice (disc) of the fuel rod is treated in the model. For fission gas release and internal gas pressure, an approximation to the whole rod is used. The slice is divided into 3 regions: cladding, gap and fuel. The fuel is subdivided by a bridging annulus into a rigid, totally cracked zone and a perfectly plastic zone, see fig. 2.1.

---

*) Fast Fuel Rod Simulator

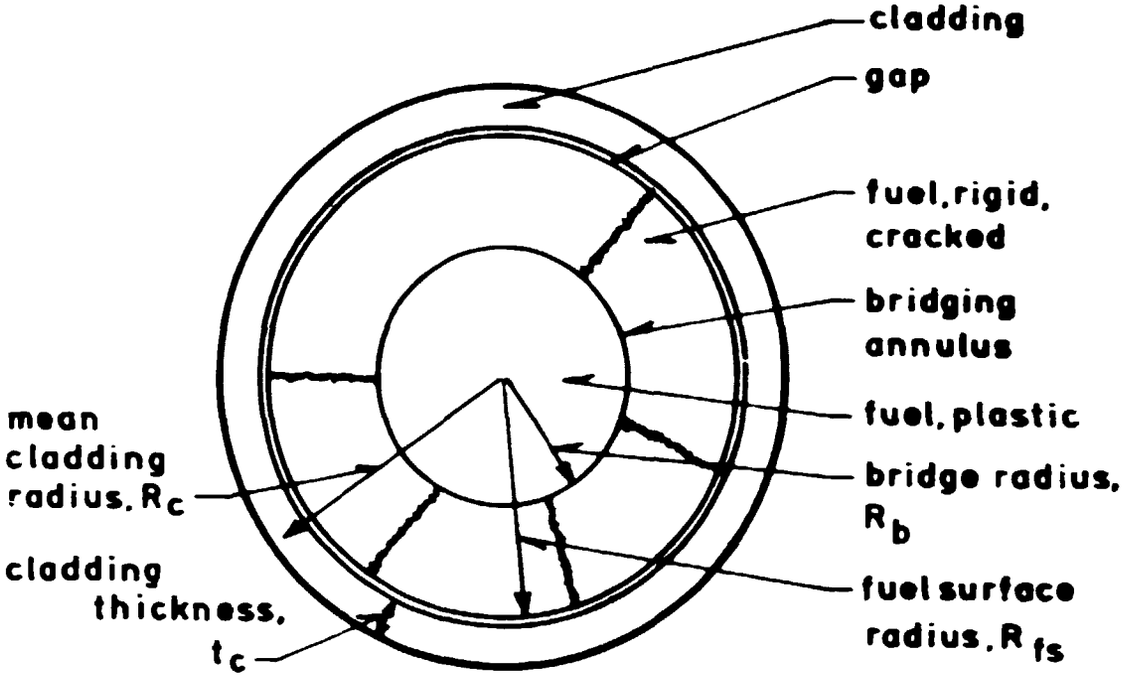

Fig. 2.1. Cross section of a fuel rod.

2.1. Cladding

2.1.1. Mechanics

The cladding is treated as an axisymmetrical, hollow, thin cylinder with an outer pressure, P_o, an inner pressure, P_i and a superimposed axisymmetrical contact pressure, P_{cp}, acting on the inside. Elastic, plastic and thermal strains are considered.

The forces acting on the cladding and the mean stresses in the cladding (σ_r, σ_t and σ_z) are shown in fig. 2.2.

The stress components $\neq 0$ in a hollow thin cylinder ($t_c << R_c$) with a pressure difference between the outside and the inside are[2)]

$$\sigma_r = P_i - P_o \quad (\text{or} \quad \sigma_r = 0)$$

$$\sigma_t = (P_i - P_o)\, R_c/t_c \qquad (2\text{-}1)$$

$$\sigma_z = (P_i - P_o)/2 \cdot R_c/t_c$$

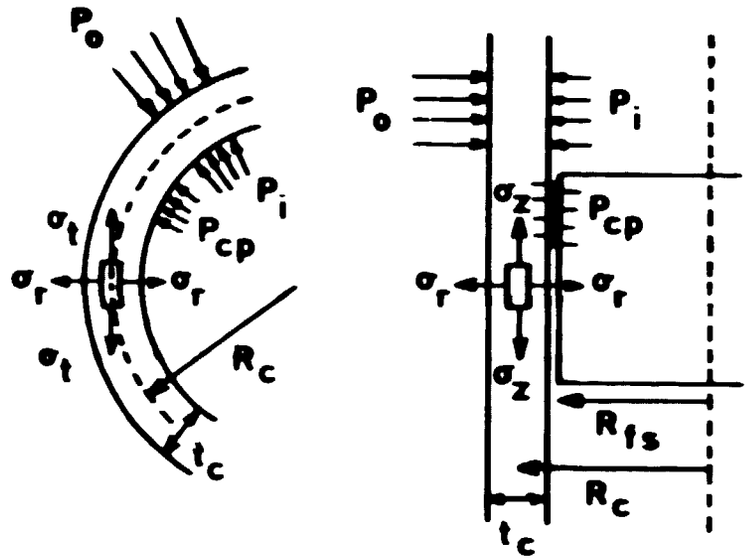

Fig. 2.2. Forces acting on and stresses in the cladding.

If an axisymmetrical contact pressure is superimposed on the cylinder sides, the stresses are

$$\sigma_r = P_i + P_{cp} - P_o \quad (\text{or} \quad \sigma_r = 0)$$

$$\sigma_t = (P_i + P_{cp} - P_o)\, R_c/t_c \tag{2-2}$$

$$\sigma_z = (P_i - P_o)/2 \cdot R_c/t_c \ .$$

According to Hooke's law, the elastic strains are

$$\varepsilon_r^{el} = (1/E)[\sigma_r - \nu(\sigma_t + \sigma_z)]$$

$$\varepsilon_t^{el} = (1/E)[\sigma_t - \nu(\sigma_z + \sigma_r)] \tag{2-3}$$

$$\varepsilon_z^{el} = (1/E)[\sigma_z - \nu(\sigma_r + \sigma_t)]$$

where E is the modulus of elasticity and ν is Poisson's ratio.

The temperature expansion of the cylinder is calculated from the cladding mean temperature, T_c

$$\varepsilon_r^{th} = \varepsilon_t^{th} = \varepsilon_z^{th} = \alpha(T_c - T_o) \qquad (2\text{-}4)$$

where α is the thermal expansion coefficient and T_o is a reference temperature.

Plastic deformations are modelled according to the simplified anisotropic theory by Hill[4]. The generalized stress, σ_g, is defined according to von Mises' yield criterion

$$\sigma_g = [(\sigma_r-\sigma_t)^2\ YG + (\sigma_t-\sigma_z)^2\ YF + (\sigma_z-\sigma_r)^2\ YH]^{\frac{1}{2}} \qquad (2\text{-}5)$$

where YF, YG and YH are anisotropic factors.

Using the mechanical material properties and the generalized stress, a generalized permanent strain, ε_g, is calculated.

The permanent strains are then

$$\begin{aligned}
\varepsilon_r^p &= \varepsilon_g/\sigma_g\ [YH(\sigma_r-\sigma_z) - YG(\sigma_t-\sigma_r)] \\
\varepsilon_t^p &= \varepsilon_g/\sigma_g\ [YG(\sigma_t-\sigma_r) - YF(\sigma_z-\sigma_t)] \qquad (2\text{-}6) \\
\varepsilon_z^p &= \varepsilon_g/\sigma_g\ [YF(\sigma_z-\sigma_t) - YH(\sigma_r-\sigma_z)]
\end{aligned}$$

The total strain, ε^t, is for each component the sum of 2-3, 2-4 and 2-6

$$\varepsilon_i^t = \varepsilon_i^{el} + \varepsilon_i^{th} + \varepsilon_i^p\ . \qquad (2\text{-}7)$$

2.1.2. Mechanical material properties

Numerical values as well as a discussion of the correlations chosen for the material properties are given in ref. 3.

E, ν and α are assumed constant independent of irradiation, deformation and temperature.

Generalized plastic strain and primary creep are calculated according to the deformation hardening hypothesis[4] with some modifications for reversed loading.

The expression for the generalized plastic strain is

$$\varepsilon_g^{pl} = (\sigma_g/K)^{1/n} \qquad (2\text{-}8)$$

where K, the stress coefficient, depends on temperature, material treatment and irradiation. n, the strain hardening coefficient, is assumed constant.

The expression for primary creep is

$$\varepsilon_g^{pr} = (\sigma_g/K)^a \, t^b \cdot \exp(-Q/(R \cdot T_c)) \qquad (2\text{-}9)$$

where K, the stress coefficient, depends on irradiation. a, b and Q are constants, R is the gas constant and t the time.

Secondary (stationary) creep is assumed to be irradiation-induced

$$\varepsilon_g^{st} = (\sigma_g/K)^a \, t \cdot \phi^d \cdot \exp(-Q/(R \cdot T_c)) \qquad (2\text{-}10)$$

where K, a, d and Q are constants; ϕ is the fluence.

The generalized permanent strain for a time step is then

$$\varepsilon_g^{p} = \varepsilon_g^{pl} + \varepsilon_g^{pr} + \varepsilon_g^{st}. \qquad (2\text{-}11)$$

2.1.3. Temperature distribution

The heat generation in the cladding is assumed negligible compared to the heat transferred through the cladding.

The temperature drop over the cladding, ΔT_c, is[5)]

$$\Delta T_c = \frac{Q \cdot \ln(R_{co}/R_{ci})}{2 \cdot \pi \cdot k_c} = \frac{Q \cdot t_c}{2 \cdot \pi \cdot R_c \cdot k_c} \qquad (2\text{-}12)$$

where Q is the heat generated in the fuel per unit length, k_c the thermal conductivity of the cladding, t_c the cladding thickness, and R_{co} and R_{ci} are the outer and inner cladding radii, respectively.

The outer cladding temperature, T_{co}, is a boundary condition. Assuming $k_c = C_o + C_1 \cdot T_c$, where T_c is the mean cladding temperature, the inner cladding temperature, T_{ci}, is

$$T_{ci} = \frac{1}{C_1} \left[- C_o + \sqrt{C_o^2 + 2 \cdot C_1 \cdot C_o \cdot T_{co} + C_1^2 \cdot T_{co}^2 + \frac{C_1 \cdot Q \cdot t_c}{\pi \cdot R_c}} \right] \qquad (2\text{-}13)$$

2.2. Fuel

2.2.1. Mechanics

The mechanical treatment of the fuel is extremely simple, only thermal expansion and creep strains are considered. Strains and temperature distribution in the fuel are axisymmetrical in the model.

2.2.1.1. Rigid region. This zone is assumed to be cracked (only compressive stresses), the thermal expansion is therefore calculated as that of a rigid bar. The temperature distribution in the outer part of the fuel, where the flux depression is small, is almost parabolic[5]. Assuming a parabolic temperature distribution and a thermal expansion coefficient, α, independent of temperature, the thermal expansion, ΔR_r^{th}, of the rigid zone is found to be

$$\Delta R_r^{th} = (R_{fs} - R_b)\,\alpha\left(\frac{T_{fs} + T_b}{6} + \frac{2}{3}\cdot T_{sb} - T_o\right) \qquad (2\text{-}14)$$

where T_{fs} is the fuel surface temperature, T_o is a reference temperature, T_b is the bridge temperature, and T_{sb} is the temperature at the midpoint between surface and bridge.

The compressive stresses are neglected because the elastic modulus of the fuel is much larger than that of the cladding.

2.2.1.2. Plastic region. The material in the plastic zone is allowed to expand freely and is assumed to be stress-free, except for hydrostatic pressure.

2.2.1.3. Bridge. A rigid annulus, the bridge, forms the boundary between the rigid and the plastic fuel zones. The position of the bridge, together with the temperature distribution in the fuel, determines the thermal expansion of the cracked pellet.

The creep deformation in the fuel changes the position of the bridge. This change in position depends on the creep strain at the bridging annulus, and the total crack opening angle, see fig. 2.3.

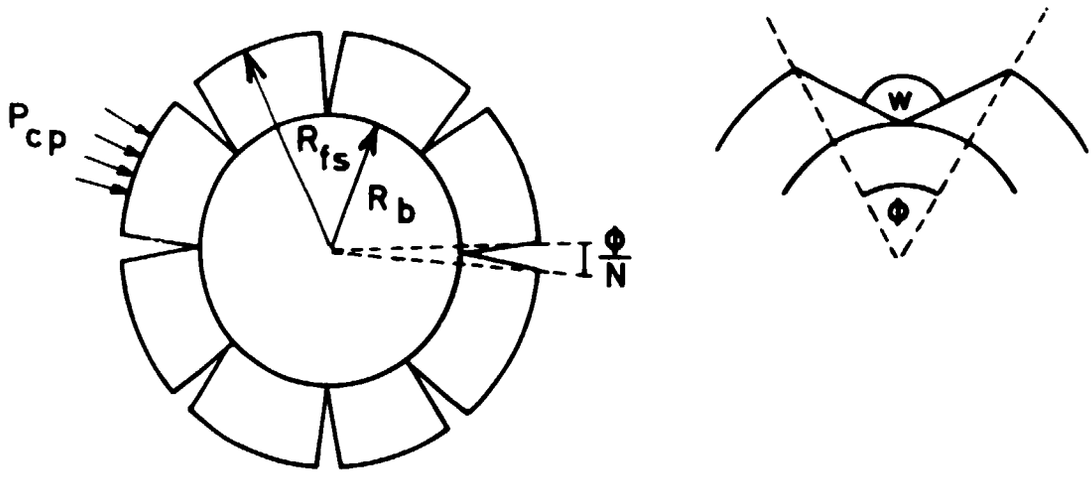

Fig. 2.3. Cracked pellet.

The stress at the bridge is:

$$\sigma_b = P_{cp} \cdot R_{fs}/R_b \qquad (2\text{-}15)$$

where P_{cp} is the contact pressure, R_{fs} the fuel surface radius and R_b the bridge radius. The UO_2 creep, ε, at the bridge is found from the bridge temperature and σ_b by the UO_2 creep equation. The area which the material from R_b to R_b + dR will occupy as a result of creep is:

$$A_{cr} = \varepsilon \cdot dR \cdot 2\pi \cdot R_b \ . \qquad (2\text{-}16)$$

The crack area between R_b and R_b + dR may be approximated by

$$A_{crk} = \pi \cdot (dR)^2 \cdot \omega/2\cdot\pi \ . \qquad (2\text{-}17)$$

Equating these areas (eqs. 2-16 and 2-17) yields the creep of the bridge:

$$dR = R_b \cdot \varepsilon \cdot 4 \cdot \pi/\omega. \qquad (2\text{-}18)$$

However, if the contact pressure is very low (or zero), and the swelling rate inside the bridge is higher than at the bridging annulus, this swelling difference will tend to open the cracks. This effect is modelled by assuming that the swelling causes a small pressure inside the bridging annulus, giving a reversed creep.

Besides closing the cracks, the creep area, A_{cr}, will slightly reduce the fuel surface radius, which is important when the cracks are almost closed.

The thermal expansion of the bridge is

$$\Delta R_b^{th} = R_b \cdot \alpha(T_b - T_o). \tag{2-19}$$

2.2.1.4. Total strain. The influence of the creep strain is only indirect through the movement of the bridge position. The total expansion of the fuel is

$$\Delta R_f = \Delta R_r^{th} + \Delta R_b^{th} + \Delta R_{sw} + \Delta R_D \tag{2-20}$$

where ΔR_{sw} is the total swelling between the bridge and the surface, and ΔR_D is the corresponding densification, described in 2.2.2.

2.2.2. Mechanical material properties

Numerical values as well as a discussion of the correlations chosen are found in ref. 3.

E and ν are not used because of the simple treatment of the fuel, and α is assumed constant independent of temperature and irradiation.

For the fuel only, secondary creep is considered. It consists of three terms: an irradiation-induced, an irradiation-enhanced, and a thermal creep term

$$\begin{aligned}\varepsilon_f = \{&K_1 \cdot \sigma_b \cdot \dot{F} \cdot \exp(-Q_1/(R \cdot T_b)) + \\ &+ (K_2 + K_3 \cdot \dot{F}) \cdot \sigma_1 \cdot \exp(-Q_2/(R \cdot T_b)) + \\ &+ K_3 \cdot \sigma_b^{a_1} \cdot \exp(-Q_3/(R \cdot T_b))\}t\end{aligned} \tag{2-21}$$

$$\sigma_1 = \min(\sigma_b, \sigma_{trans}); \quad \sigma_{trans} = K_4 \cdot G^{a_2}$$

where K_1, K_2, K_3, K_4, Q_1, Q_2, Q_3, a_1 and a_2 are constants, σ_b and T_b the stress and the temperature in the fuel, G the grain size of the fuel, and $\dot{F}$ the fission rate.

Densification is modelled according to the theory proposed by Stehle and Assmann[6].

The densification is isotropic and independent of temperature and stress and therefore uniformly distributed. The expression for densification is

$$(\Delta V/V)_{Dens} = - \sum_{i=1}^{n} P_i \left[1 - \left(1 - \frac{W_{eff} \cdot \lambda \cdot F}{3 \cdot r_i}\right)\right] \qquad (2\text{-}22)$$

$$\Delta R_D = 1/3 \cdot (\Delta V/V)_{Dens}$$

P_i = the porosity of pores with radius r_i
λ = the range of a fission fragment
W_{eff} = the volume of a pore that is atomized into vacancies when a fission fragment traverses a pore
F = burn-up, n = number of pore groups.

W_{eff} can be considered an empirical parameter which is then fitted to experimental data.

Low temperature swelling (matrix swelling, solid swelling) is assumed to vary linearly with burn-up. Gaseous fission product swelling is considered in the temperature region 1000-2000°C; the expression for gaseous fission product swelling is

$$(\Delta V/V)_{sw} = \min\{K_{sw}(T) \cdot F, K_{max}(r_g)\} \qquad (2\text{-}23)$$

$$K_{sw}(T) = ((T - 1000^{\circ}C) \cdot K)^3 \qquad 1000 < T < 2000^{\circ}C$$

K = a constant
K_{max} = a constant dependent on the fuel structure (fuel grain size) and perhaps temperature
F = burn-up.

The calculation of swelling is performed in a number of annuli. The total expansion due to swelling is

$$\Delta R_{sw} = \left\{ \sum_{i=1}^{m} (\Delta V/V)_{sw} \cdot \frac{1}{3 \cdot m} + F \cdot K_{swl} \cdot 1/3 \cdot R_{fs} \right\} \qquad (2\text{-}24)$$

m = number of annuli in the swelling calculation
F = burn-up
K_{swl} = solid swelling rate.

Swelling is assumed to be isotropic.

2.2.3. Temperature distribution

The temperature distribution in a solid cylindrical rod with internal heat generation from fission, and subject to flux depression, is found by solution of the equation[7)]

$$\int_{T_{fs}}^{T_r} k_f(T)\, dT = \frac{Q}{4 \cdot \pi} \frac{I_o(\kappa \cdot R_{fs}) - I_o(\kappa \cdot r)}{1/2 \cdot \kappa \cdot R_{fs} \cdot I_1(\kappa \cdot R_{fs})} \qquad (2\text{-}25)$$

T_{fs} = temperature at the fuel surface, boundary condition
T_r = temperature at radius r
$k_f(T)$ = thermal conductivity of the fuel at temperature T
Q = heat rate per unit length of the fuel rod
κ = inverse neutron diffusion length
I_o, I_1 = Bessel functions.

Since $k_f(T)$ is a complicated function, eq. 2-25 is solved numerically. Equation 2-25 can be solved for either T_r or r, given the other value.

The expression for $\int_o^{T_1} k_f(T)\, dT$ is given in ref. 3.

2.2.4. Fission gas

In the fuel a number of gas atoms are produced for each fission; in a thermal flux the number is ≈ 0.31 atoms per fission[8)].

The number of fissions per meter rod is

$$Q/(EFIS \cdot 1.602 \cdot 10^{-13})$$

where EFIS is the energy produced per fission. Multiplying by 0.31 and dividing by the Avogadro number yields the number of mol produced per meter rod per s. Multiplying by 3600 (seconds per hour) and 22.4×10^{-3} (volume of a mol under standard conditions) yields the amount of fission gas in m^3 produced per meter per h. Multiplying by L_{eq} and the step time, t_i, yields the amount of fission gas produced in the rod in this time step

$$FG_i = 0.31 \cdot Q \cdot L_{eq} \cdot t_i \cdot 3600 \cdot 22.4 \cdot 10^{-3} / (6.023 \cdot 10^{23} \cdot EFIS \cdot 1.602 \cdot 10^{-13}). \quad (2\text{-}26)$$

L_{eq} is the active length of the rod multiplied by the ratio between average rod power and actual pellet power. L_{eq} is introduced to obtain a correct fission gas release for the whole rod based on the calculation at a single axial location.

The release of fission gas is modelled according to an empirical model. The release fraction corresponding to a given temperature distribution is

$$X_n = (F_1 \cdot V_1 + F_2 \cdot V_2 + \cdots + F_m \cdot V_m) \quad (2\text{-}27)$$

F_j is the release fraction valid in the temperature interval from T_{j-1} to T_j and V_j is the volume fraction of the pellet with temperature in the interval from T_{j-1} to T_j.

The amount of fission gas released at time step n is[9)]

$$R_n = \max\{(X_n \cdot \sum_{i=1}^{n} FG_i - \sum_{i=1}^{n-1} R_i), 0\}. \quad (2\text{-}28)$$

Numerical values can be found in ref. 3.

For very high burn-up (above 20.000 MWD/t UO_2), the correction proposed by Meyer[10)] is used.

2.3. Gap conductance

The connection between fuel and cladding is the gap.

The gap conductance for an axisymmetrical open gap is

$$h_{gs} = \frac{k_{mix}}{g + \Delta X} \quad (2\text{-}29)$$

where g is the physical separation of fuel and cladding, ΔX depends on the temperature jump distances and the surface roughnesses, and k_{mix} is the thermal conductivity of the gas in the fuel rod (in the gap).

The experimentally measured gap conductances for fuel rods show large deviations from this formulation. Several correlations have been proposed in order to obtain better agreement between experiments and calculations.

The correlations proposed by Kjærheim and Rolstad[11] and by Vitanza[12] are both based on the assumption that even when the calculations predict a gap between fuel and cladding, part of the fuel is in contact with the cladding.

The correlation proposed by Vitanza[12] is used in FFRS. The area in contact is, for the eccentric situation,

$$A_c = \max\{[1-(gap/(gap_o - A_o))^{1.5}], 0\} \qquad (2\text{-}30)$$

where gap_o is the cold gap and A_o is a constant.

When the gap is closed, the gap conductance is based on the model proposed by Ross and Stoute[13]

$$h_{gc} = \frac{k_{mix}}{\Delta X} + H_1 \cdot P_{cp} , \qquad (2\text{-}31)$$

H_1 is a constant depending on the thermal conductivity of fuel and cladding, the surface roughnesses and the yield strength of the cladding, P_{cp} is the contact pressure.

By combining 2-29 and 2-31, the gap conductance is

$$h_g = A_c \cdot \frac{k_{mix}}{\Delta X} + (1 - A_c) \frac{k_{mix}}{g + \Delta X} + H_1 \cdot P_{cp} . \qquad (2\text{-}32)$$

2.4. Internal pressure

The gas contained in the fuel rod consists of fill gas, R_f, released fission gas, R_{fg}, and perhaps some residual gas, R_r, released from the fabrication process. This gas is contained in the volume V_p, which consists mainly of the plenum volume. The plenum gas temperature, T_G, is almost equal to the outside cladding temperature (the coolant temperature), T_{co}. Assuming ideal gasses, the internal pressure in the fuel rod is

$$P_{in} = \frac{R_{fg} + R_f + R_r}{V_p} \cdot \frac{T_G + 273}{273} \cdot P_o \cdot \qquad (2\text{-}33)$$

R_f, R_{fg} and R_r are volumes at 0^oC and the pressure P_o.

3. THE TIME-DEPENDENT QUASI-STATIONARY MODEL FOR A FUEL ROD

3.1. The stationary solution

The equations in chapter 2 describe the stationary temperature, stress and strain distribution in fuel, gap and cladding, including some changes in the materials with burn-up and time.

As the temperature distribution within each region is independent of the stress and strain distributions, the solution for a fixed time step can be found directly for each region, given some boundary conditions.

The gap conductance, as well as the contact pressure, depends on the stress and the strain distributions in fuel and cladding. The temperature distribution in the fuel depends on the gap conductance. The common stationary solution for the fuel rod is therefore found by simultaneous solution of the equations with the given boundary and initial conditions for the fuel rod. The boundary and initial conditions are, for example, outer cladding temperature, heat load, pressure (outer and inner), cold geometry and material conditions.

The solution is found iteratively with the gap condition (gap conductance, gap size and contact pressure) as parameter. Figure 3.1 shows the solution schematically.

The stationary model as outlined in fig. 3.1 includes creep in cladding and fuel; but the solution is found for a fixed time step, and therefore the creep deformation is treated as a time-independent plastic deformation.

This part of the model can be refined to include different time-dependent effects, but does not treat a detailed irradiation history, which will often be very important for a fuel rod.

There are numerous models possessing approximately these characteristics; the oldest are probably the British[14] and the Canadian[15] models. The best known code of this type today is CAPCON THERMAL[16], a code developed for the American Nuclear Regulatory Commission.

3.2. The path dependent model

The simulation of a realistic irradiation case requires consideration of time-dependent boundary conditions as well as

changes in the materials with time. Therefore the simple model described in sec. 3.1 was extended to a path-dependent fuel model, Fast Fuel Rod Simulator, FFRS.

3.2.1. Constant heat load

During a period with constant heat load, the most important changes arise from creep and changes in the material conditions such as swelling, densification and fission gas release.

The solution is essentially obtained by an incremental theory; the temperature distribution from the last time step is used in the evaluation of swelling and fission gas release during the time step considered. In order to stabilize the time

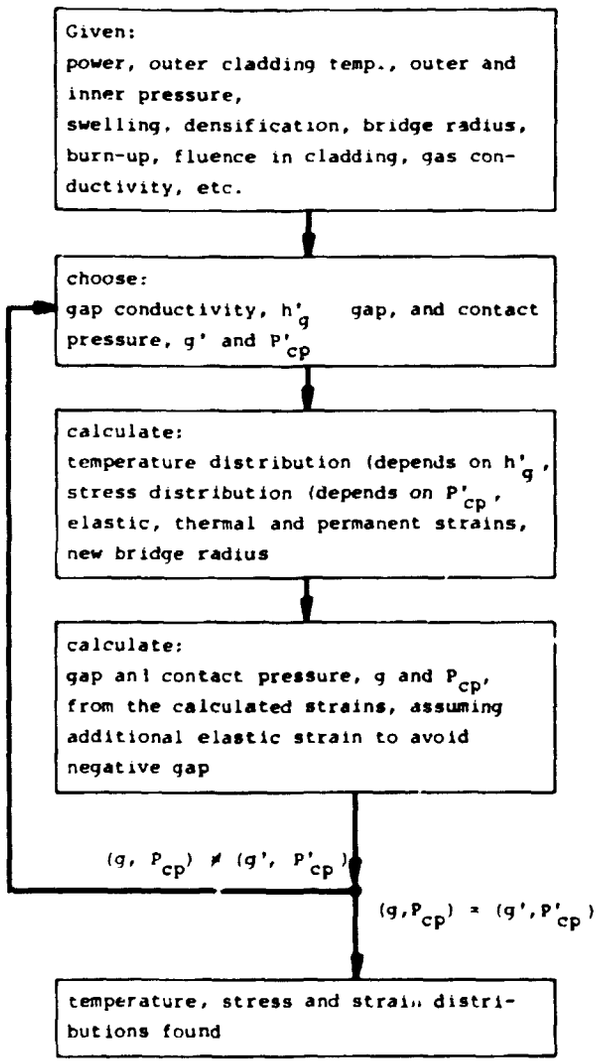

Fig. 3.1. Solution of the stationary equations.

integration even when very large time steps are used, average stress, strain and temperature distributions are found for the time steps as shown in fig. 3.1.

Fission gas release and swelling are not included in the iterative solution, but are based on values from the preceding time step. This considerably reduces the computational work by avoiding a detailed calculation of the fuel temperature distribution during the iterations.

In the calculation of the bridge movements (fuel creep), the former bridge position and temperature are used as the initial values for the evaluation of the fuel creep rate. This approximation simplifies the calculations; but it can be a significant simplification, if the time steps are long, since the temperature gradient in the fuel is high.

These two simplifications have an important influence on the length of the time steps that can be used; but if the step length is small enough (approaches zero), the simplifications introduce no additional approximations in the model.

3.2.2. Power changes

When the heat load is raised during a power ramp, the thermal expansion is larger for the inner parts of the fuel than for the outer. This will stress the outer part of the fuel in tension and thereby crack it. If the power ramp is "large", the pellet will crack up to the centre, but contact between fuel and cladding can again, by creep, close the cracks in the hottest part of the fuel. The radius, until the position at which the cracks open, is defined as the bridging annulus in the model.

After contact is made between fuel and cladding, the bridge position will be determined by a balance between the different thermal expansions and the creep rate near the bridge. This balance is found as follows:

The power ramp is divided into "small" ramps. In each "small" ramp the bridge is moved a fraction of the pellet radius towards the centre, then the bridge is allowed to creep back, as far as the creep rate (at the new bridge position) and the time allow.

During a fall in heat load the bridge position is assumed

unchanged in the model. Physically, the cracks will close in the outer parts and cracks will open in the inner parts. The cracks inside the bridging annulus can provide space for thermal expansion in a new ramp. The bridge position therefore remains unchanged during a ramp until the power reaches the former maximum power.

If the fuel operates for some time at the reduced power level, some of the internal crack volume is filled by swelling and relocation. The power level at which the thermal expansion again starts moving the bridge towards the centre is thereby lowered. As compensation for swelling and relocation, this power level is decreased linearly with burn-up until the actual power is reached.

The quasi-stationary path-dependent model is shown schematically in fig. 3.2.

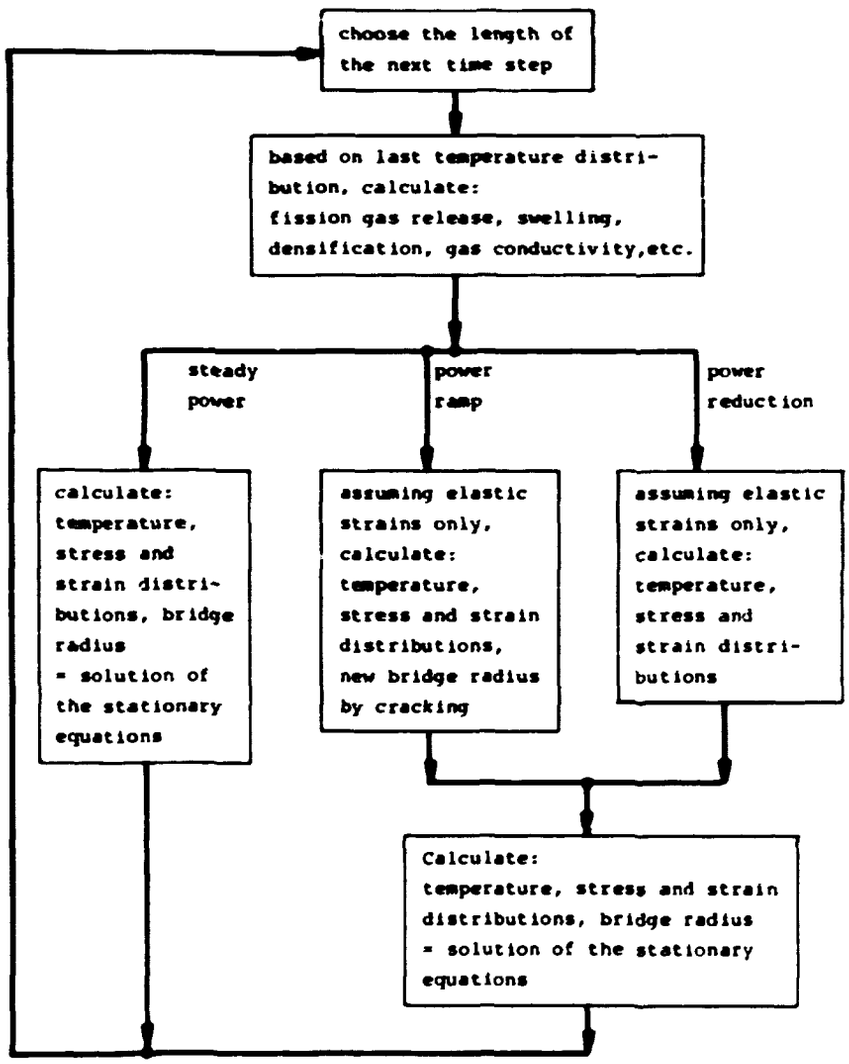

Fig. 3.2. The time-dependent, quasi-stationary model FFRS.

4. INFLUENCE OF THE PHYSICAL AND NUMERICAL APPROXIMATIONS IN FFRS

The physical description of the fuel rod (the model) is very simple so as to allow for fast computer calculation. Only comparisons with experiments, or perhaps more advanced fuel modelling codes, can determine whether these approximations are reasonable or not.

Besides the simplifications in the stationary model, the treatment of a time-dependent irradiation case includes some approximations, the influence of which can be investigated by means of the model itself. These approximations have led to the two semi-empirical parameters, Q_{burn} and Q_{ref}.

Q_{burn} = the inverse of the rate at which the power level where crack opening starts is decreased,

Q_{ref} = the power change that will crack the pellet.

Additional numerical approximations are included, since the time steps are not infinitely small, and the iterative solutions involved are stopped at finite accuracy.

The influence of Q_{burn}, Q_{ref}, and the numerical approximations is illustrated in this chapter.

4.1. The parameter Q_{burn}

Q_{burn} is a measure for how fast the fuel relocates after a fall in power. A new rise in power is not assumed to crack the fuel or to open closed cracks, until the former maximum power is exceeded. This power level, Q_{max} (where cracking starts) is reduced by $\Delta Q_{max} = \Delta Burnup/Q_{burn}$, until the power level at that moment is reached.

In the model the normally used value for Q_{burn} is $0.5 \cdot 10^{-6}$ ppm · m/W, corresponding to $\Delta Q_{max} = 200$ W/cm after 8 months at 400 W/cm.

Originally, it was planned to fit Q_{burn} to experimental results or to fuel modelling codes with a detailed treatment of the fuel region, but the influence of Q_{burn} has been shown to be quite small. Unless extreme values are used for Q_{burn}, the difference in the predicted results is much less than the uncertainty due to the possible variation in the material properties.

The influence of Q_{burn} is illustrated by calculations on an irradiation experiment[17] (irradiation: HP 013/055; Pin: M20-1B; Danish). This experiment was chosen for its high burn-up and large number of small power changes.

The influence of the uncertainty in material properties is illustrated by the difference between two calculations with different assumptions for the cladding texture. The cladding tube is either assumed to be isotropic or anisotropic with the anisotropy factors from ref. 18. The calculation in which isotropy of the cladding is assumed is the most sensitive to changes in Q_{burn} (and other parameters). Therefcre calculations are performed with $Q_{burn} = 0.1 \cdot 10^{-6}$ ppm · m/W and $Q_{burn} = 2.5 \cdot 10^{-6}$ ppm · m/W for this case.

In fig. 4.1 the calculated tangential strain is shown versus the irradiation time. The tangential stress during the final ramp is shown in fig. 4.2. For the rest of the irradiation, the differences in the calculated tangential stresses are small.

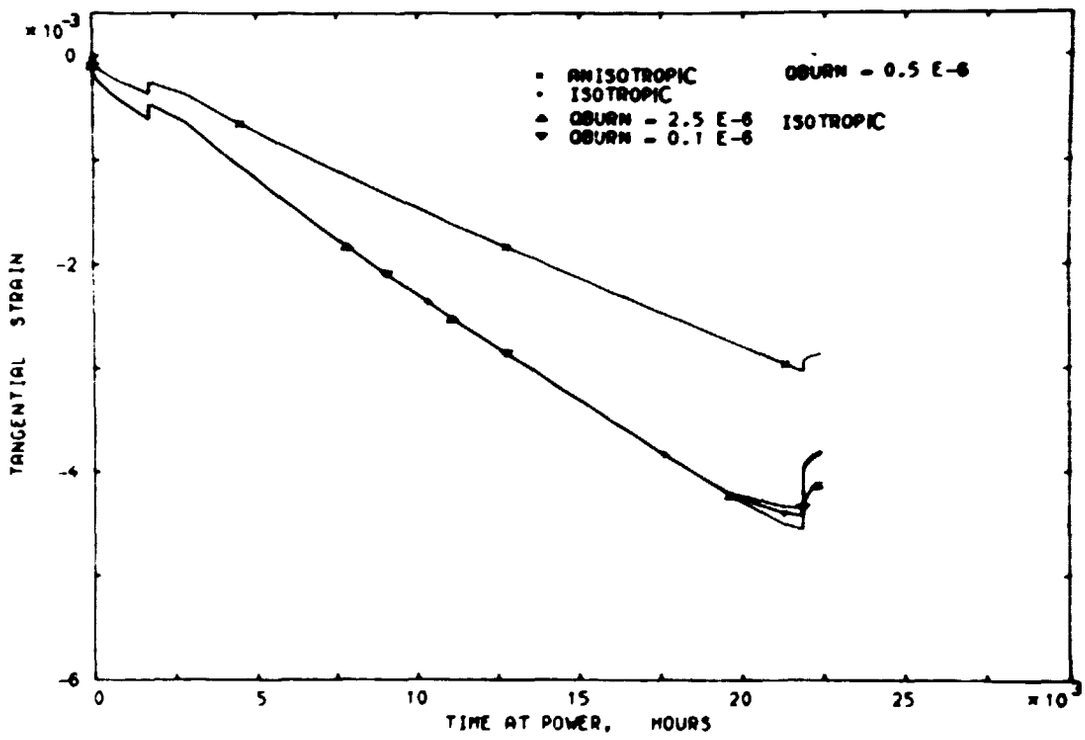

Fig. 4.1. Influence on the calculated tangential strain of the parameter Q_{burn}, compared with the influence of cladding texture, a typical material uncertainty. Pin: M20-1B.

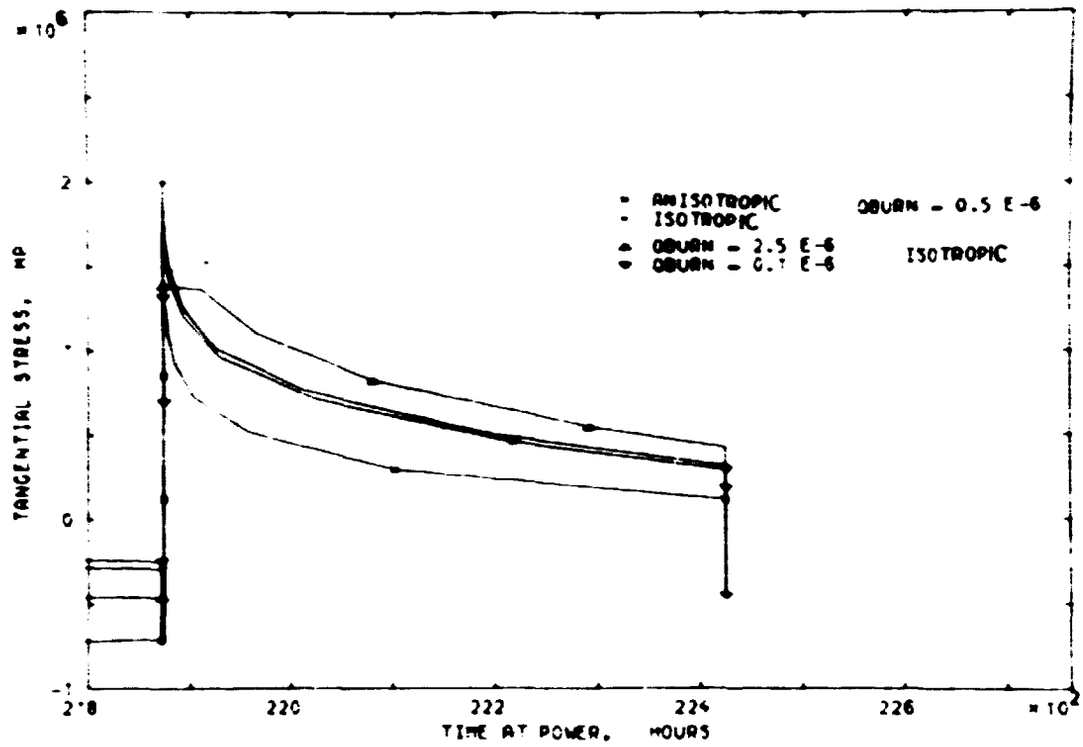

Fig. 4.2. Influence on the calculated tangential stress of the parameter Q_{burn}, compared with the influence of cladding texture, a typical material uncertainty. Pin: M20-1B.

The conclusion from this example, where a variation of Q_{burn} with as much as a factor of 25 had very little effect on the calculations, is that it is neither possible nor necessary at the moment to draw any conclusions about Q_{burn} from the experimental results. And from observing the large deviations between code predictions on well-characterized benchmark cases (refs. 18 and 19), it is obvious that state-of-the-art fuel models cannot either be used to "tune" a parameter such as Q_{burn}.

4.2. The parameter Q_{ref}

From the definition of Q_{ref} it is possible to put some limitations on the numerical value. A large, fast power increase ($\geq$ 500 W/cm) is assumed to crack the fuel totally, and a small increase in power ($\leq$ 50 W/cm) is not expected to have this marked effect. It is therefore reasonable to seek the value of Q_{ref} in the interval from 50 to 500 W/cm.

The sensitivity of the model with regard to Q_{ref} was investigated by calculations on a single power ramp. Fuel rod design and irradiation conditions are taken from a Canadian ramp experiment[19] (Pin X-264). Comparison between some fuel modelling codes, including FFRS, and the experimental results can be found in ref. 20.

Figure 4.3 shows the calculated strain (elastic + permanent) as a function of the heat load for different values of Q_{ref}. The value of ΔP, which determines the step length during a power ramp, is chosen very small to reduce the numerical influence on the results. The figure clearly demonstrates that the value of Q_{ref} has very little effect on the modelling of a large power ramp. A value of 200 W/cm is chosen for Q_{ref}.

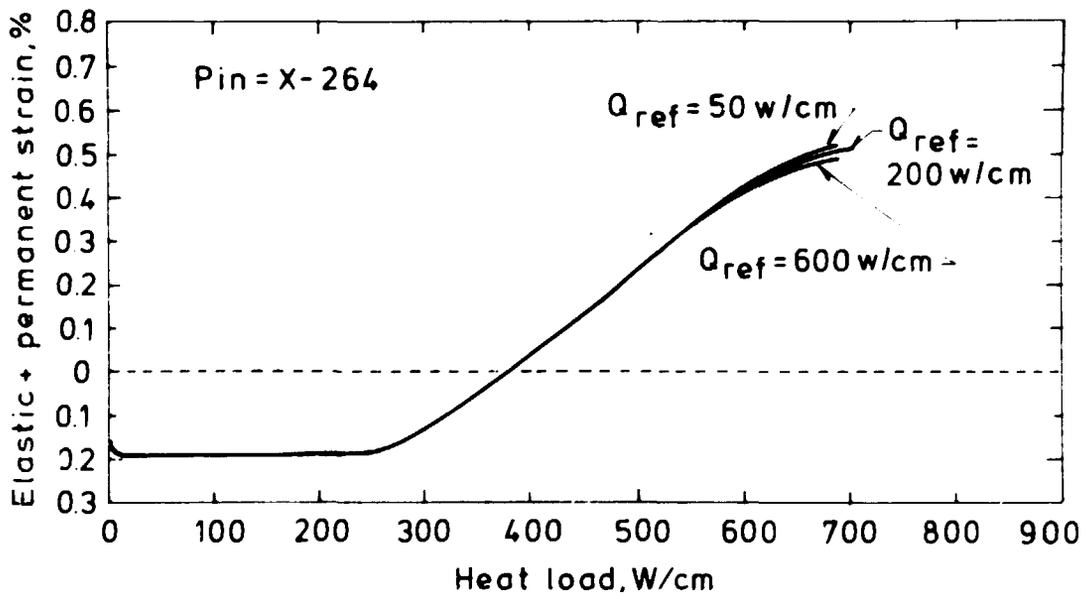

Fig. 4.3. Calculated strain as a function of heat load for different values of the parameter Q_{ref}. Pin: X-264.

4.3. The step length during a power ramp

For the value of Q_{ref} chosen, the influence is investigated of the step length (proportional to ΔP).

In fig. 4.4 the calculated strain (elastic + permanent) is shown for different values of ΔP. A value of ΔP = 10 W/cm yields, for this ramp, a reasonable compromise between the calculation time and the accuracy. For all other irradiation experiments calculated with FFRS, a value of 20 W/cm for ΔP gave

no difference in the calculated strains compared to smaller values for ΔP. The reason for this is the high fuel temperatures (high heat load) calculated for the X-264 pin.

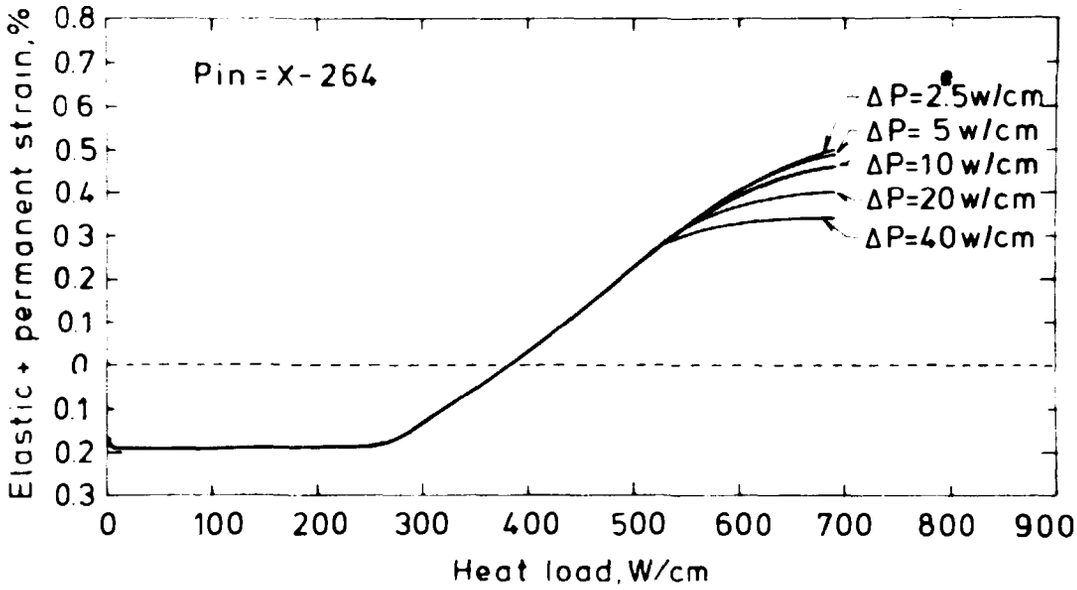

Fig. 4.4. Calculated strain as a function of heat load for different values of ΔP, the step size in power ramps. Pin: X-264.

4.4. Influence of the time increments during constant power operation

As explained in chapter 3, the model FFRS is essentially an incremental model, where the calculated stress, strain and temperature distributions from the preceding time step are used in the calculations of fuel creep, swelling and fission gas release. This necessitates small time steps, when fuel creep, hot swelling and fission gas release are important. On the other hand, the most sensitive property, the gap conductance, is found as an average value for the time step by iteration, as shown in fig. 3.1. Therefore the time steps can be quite large without affecting the average values for a time period, when fuel creep, hot swelling and fission gas release are moderate.

Since fission gas release and hot swelling are only important at elevated temperatures, the length of the next time step is determined on the basis of the fuel centre temperature, T_c, and a given maximum step length, Δt_{max}, as $\Delta t_{next} = f(\Delta t_{max}, T_c)$.

If there is contact between fuel and cladding, the bridge movements are estimated on the basis of the contact pressure at that moment. The time step is then chosen so that the estimated bridge movements are below $\Delta R_b \cdot R_{fs}$ in the time step. ΔR_b is a given maximum fraction of the fuel radius that the bridge may move in a time step.

As the purpose of developing FFRS was to have a fast fuel model, the time steps were not to be chosen too small. The standard values for Δt_{max} and ΔR_b are 2500 hours and 5%.

The influence of this choice is illustrated by calculations with different values of Δt_{max} and ΔR_b on the HP 013/055 irradiation experiment.

Figures 4.5 and 4.6 show the influence of Δt_{max} on the tangential strain and the tangential stress in the final ramp.

Figures 4.7 and 4.8 show the influence of ΔR_b.

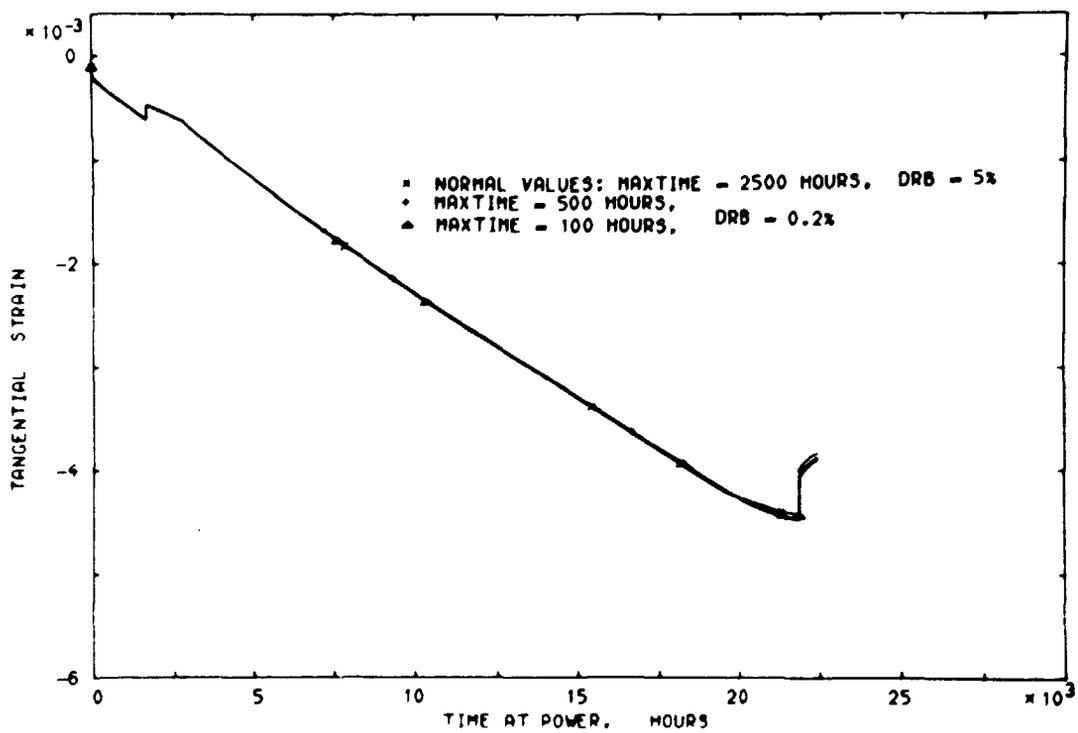

Fig. 4.5. Influence of the chosen time increments (proportional to MAXTIME) on the tangential strain. Pin: M20-1B.

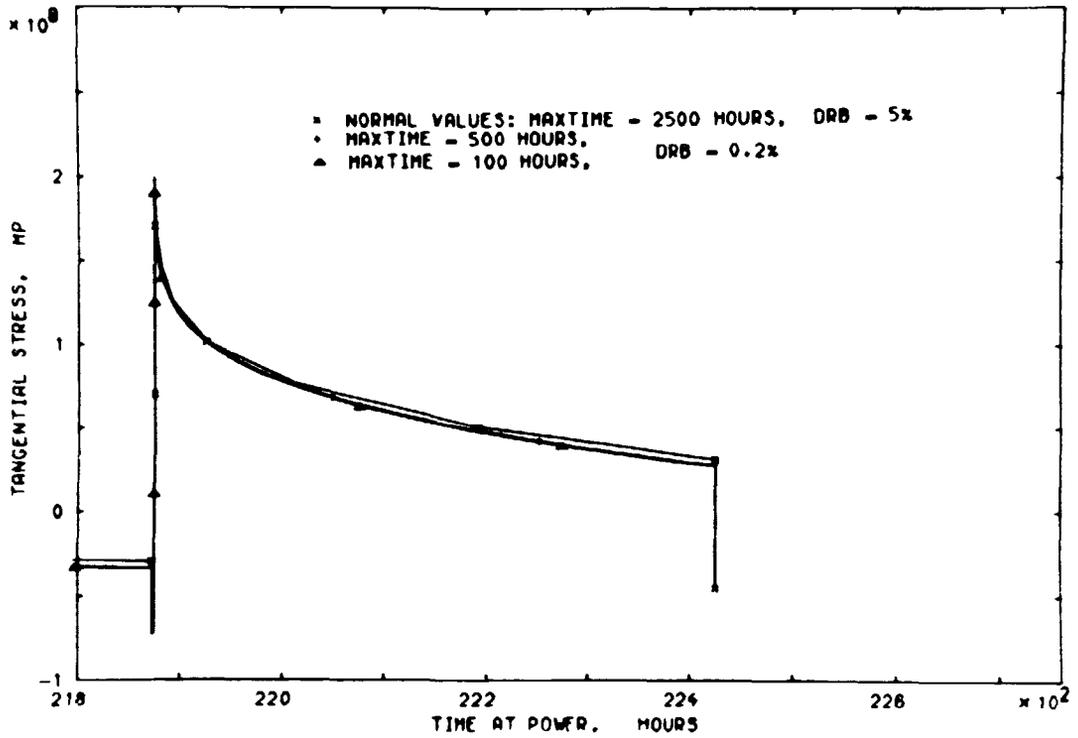

Fig. 4.6. Influence of the chosen time increments (proportional to MAXTIME) on the tangential stress. Pin: M20-1B.

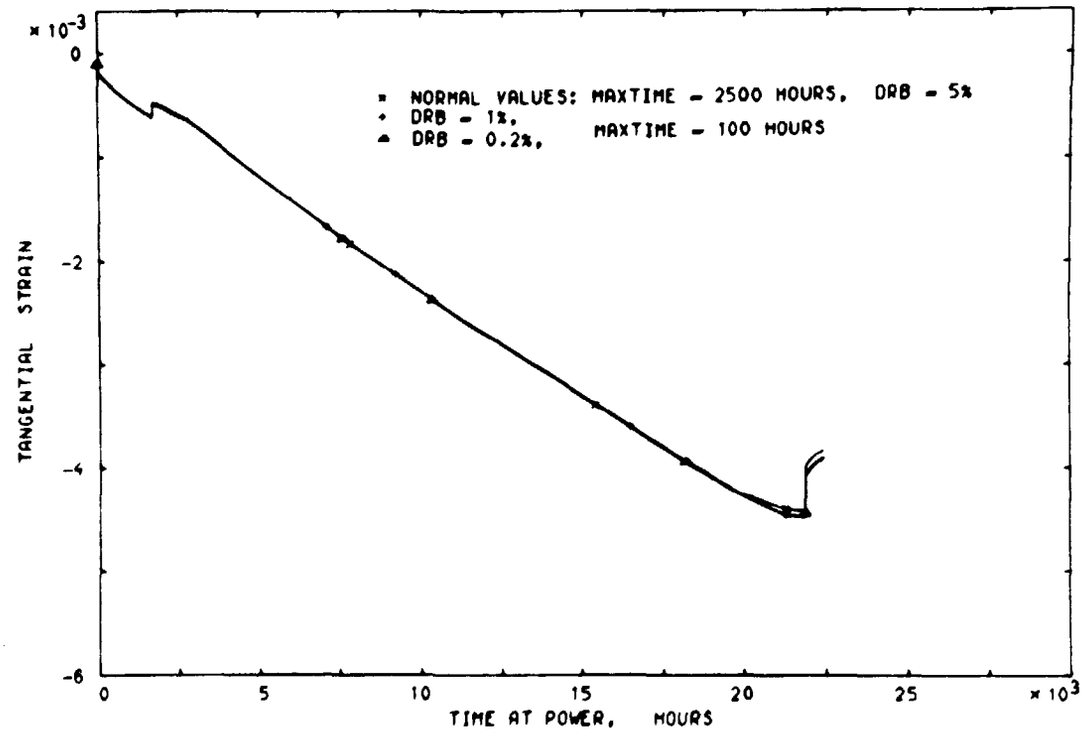

Fig. 4.7. Influence on the tangential strain of the time increment size during contact between fuel and cladding. Pin: M20-1B.

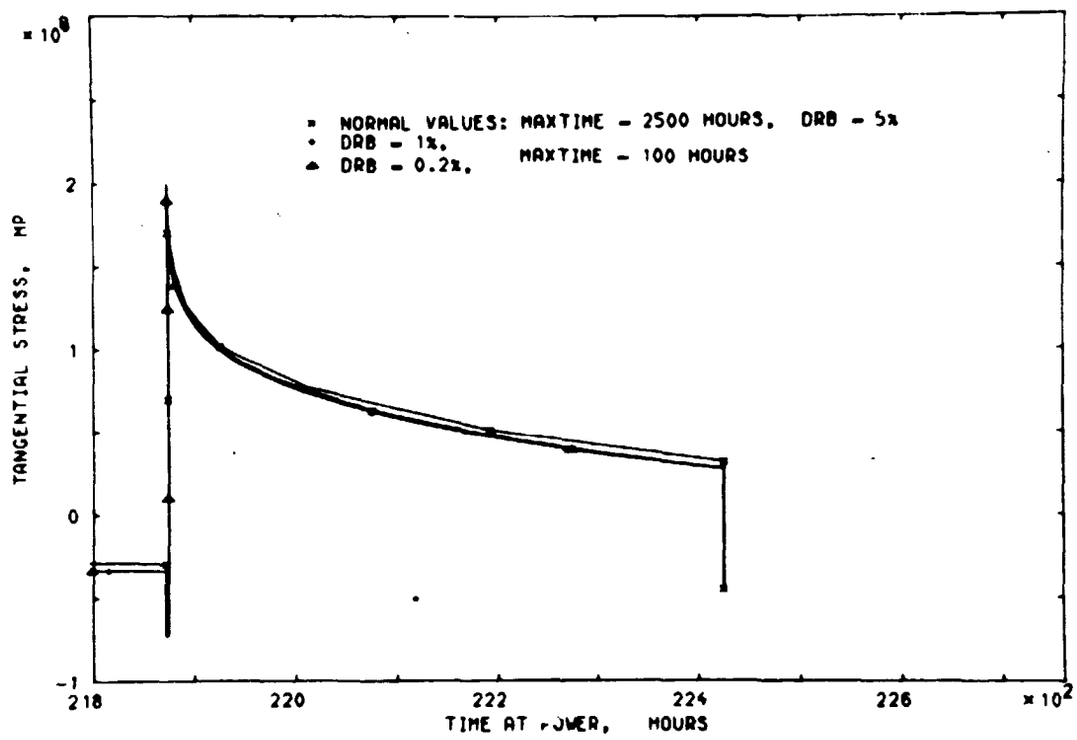

Fig. 4.8. Influence on the tangential stress of the time increment size during contact between fuel and cladding, Pin: M20-1B.

4.5. Accuracy in the iterations

As the stop criterion in the iterative solution of the stationary equations (fig. 3.1) and the equation for heat conduction in the fuel, 1% accuracy is normally used. Calculations with the stop criterion set to either 10% or 0.1% give differences that are below 4% in the tangential stress and strain.

5. PERFORMANCE OF FFRS

5.1. General behaviour of the model

The general behaviour of the model is best illustrated through the simulation of a couple of irradiation experiments. The values for some of the parameters describing the fuel situation are shown in figs. 5.1-5.9. The experiments chosen are the Canadian X-264 rod[19] and a commercial PWR rod[19]. Calculations performed with a number of fuel codes can be found for both rods in ref. 19.

The X-264 fuel rod was ramped to a high power without pre-irradiation. The case therefore illustrates the mechanical interaction during a power ramp, where any effect of densification, hot swelling and relocation is negligible. For this case, fig. 5.1 shows the fuel centre, the bridge and the fuel surface temperatures, 5.2 the fuel to cladding contact pressure, 5.3 the total tangential strain in the cladding, and 5.4 the tangential stress in the cladding.

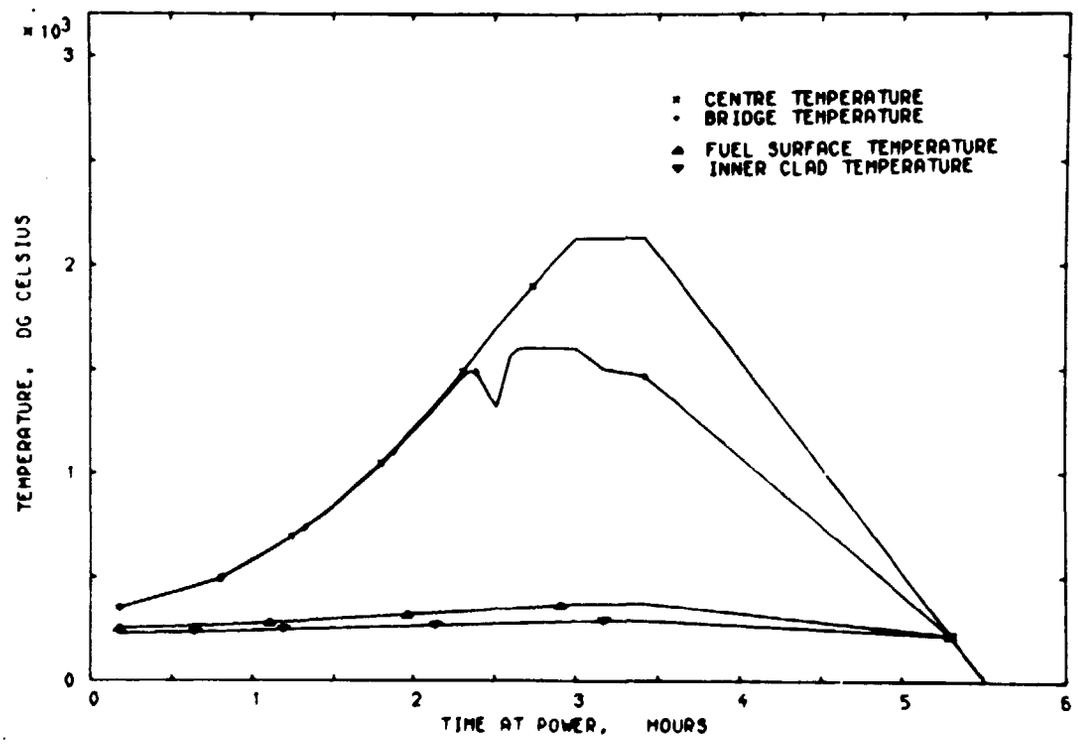

Fig. 5.1. Calculated temperatures for the X-264 fuel pin.

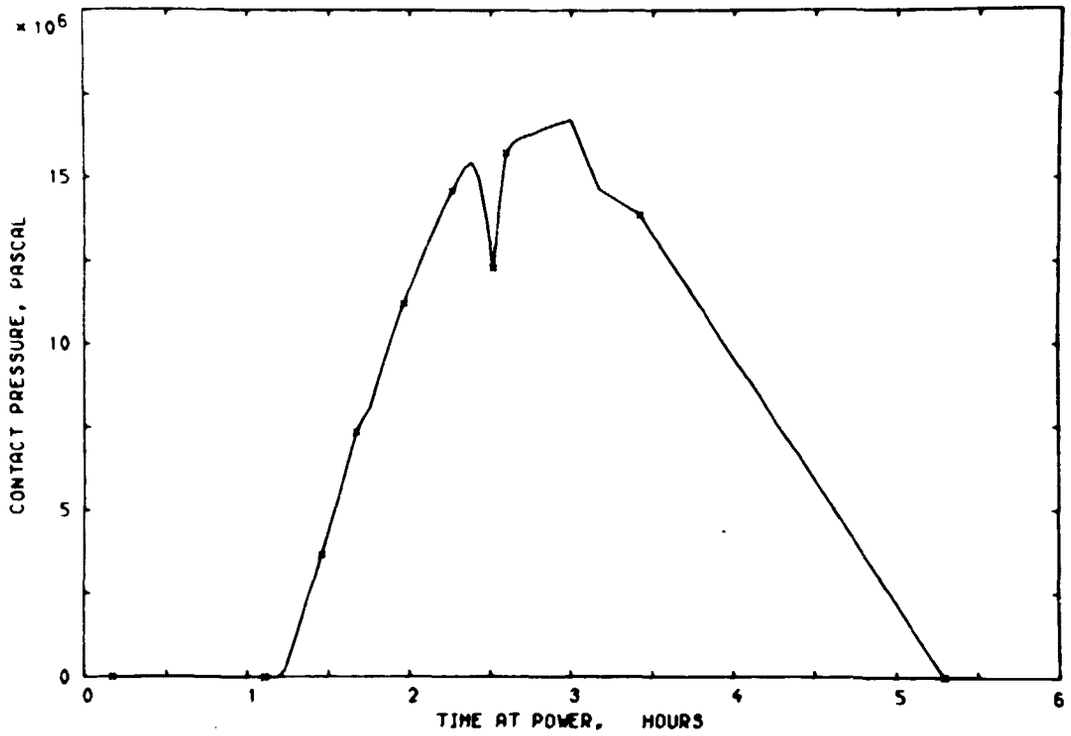

Fig. 5.2. Calculated contact pressure between fuel and cladding for the X-264 fuel pin.

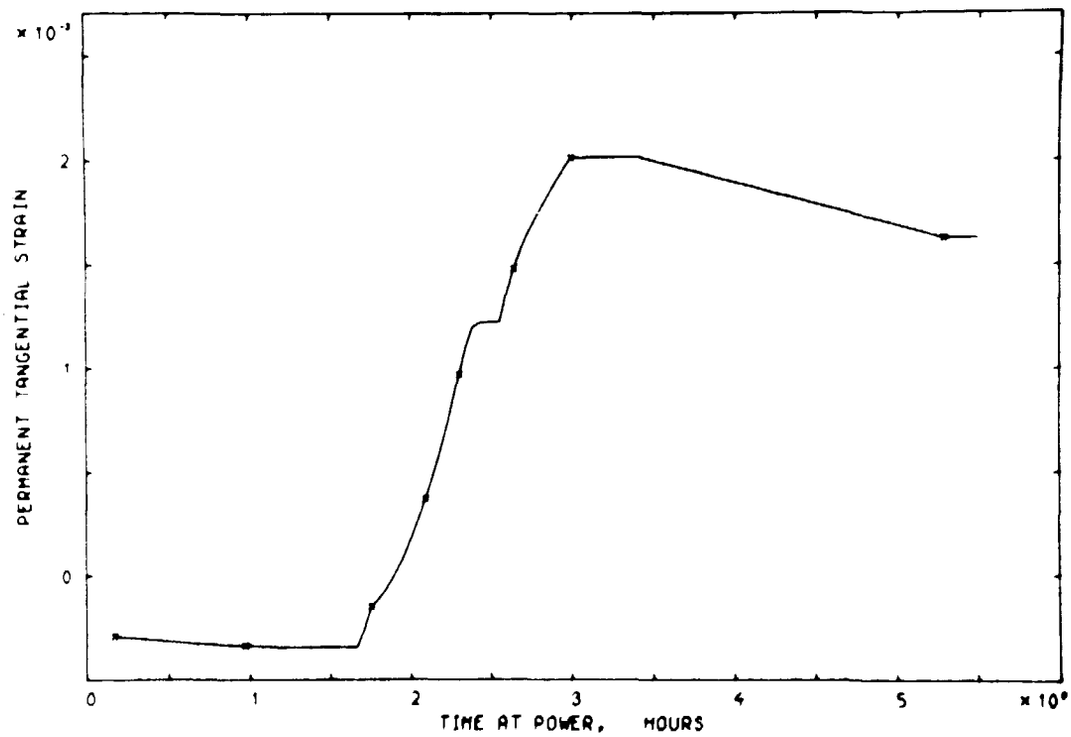

Fig. 5.3. Calculated permanent tangential strain for the X-264 fuel pin.

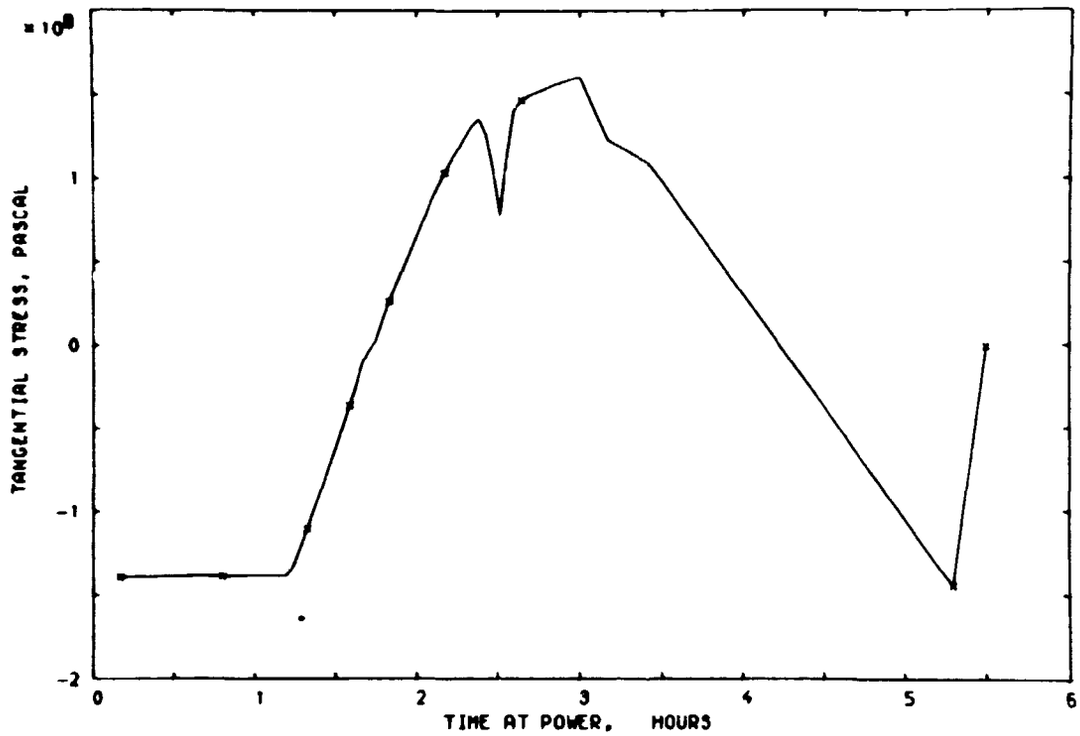

Fig. 5.4. Calculated tangential stress for the X-264 fuel pin.

The commercial PWR rod is of a type with unstable fuel (large and fast densification) and without pre-pressurization. The fast densification at the beginning of the irradiation results in a very large gap between fuel and cladding, this leads to high temperatures in the fuel. The high fuel temperatures are followed by fission gas release (raising the temperatures) and hot swelling (lowering the temperatures by closing the gap). This case illustrates the interaction between densification, hot swelling and fission gas release; it is, however, very sensitive to changes in design and material properties, and thus the numerical results shown should be considered with some reservation. The parameters shown in figs. 5.5 to 5.9 as functions of time are heat load, temperatures, hot gap, gap conductance and amount of fission gas released.

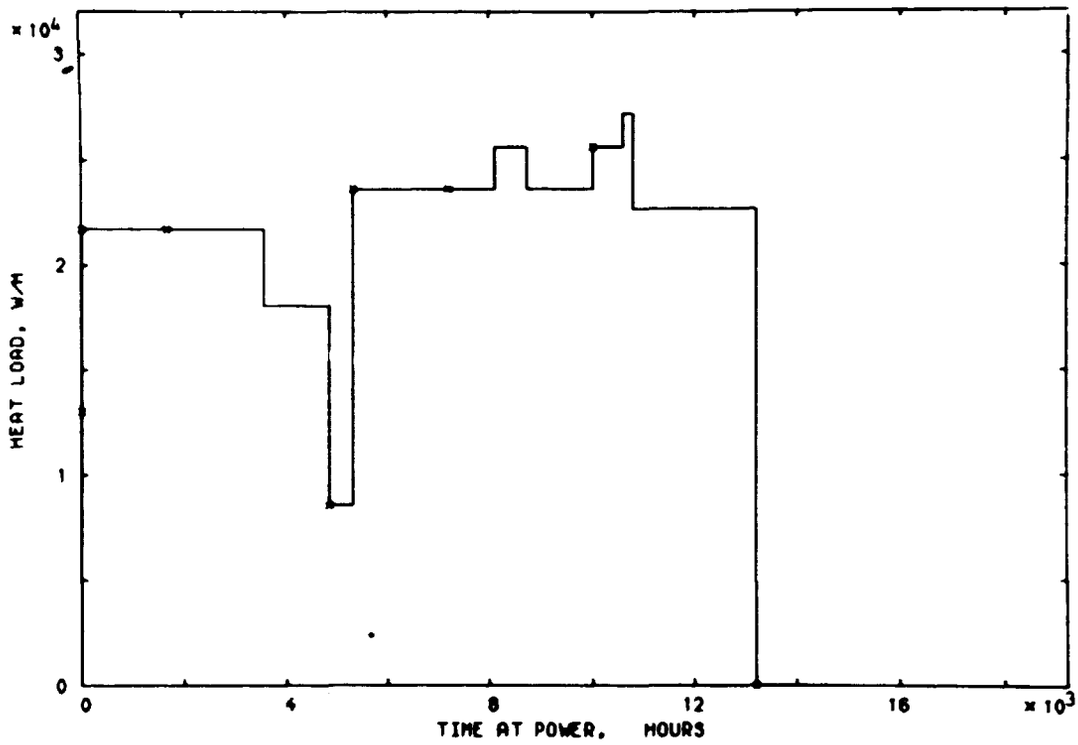

Fig. 5.5. Heat load as a function of time for the PWR fuel rod.

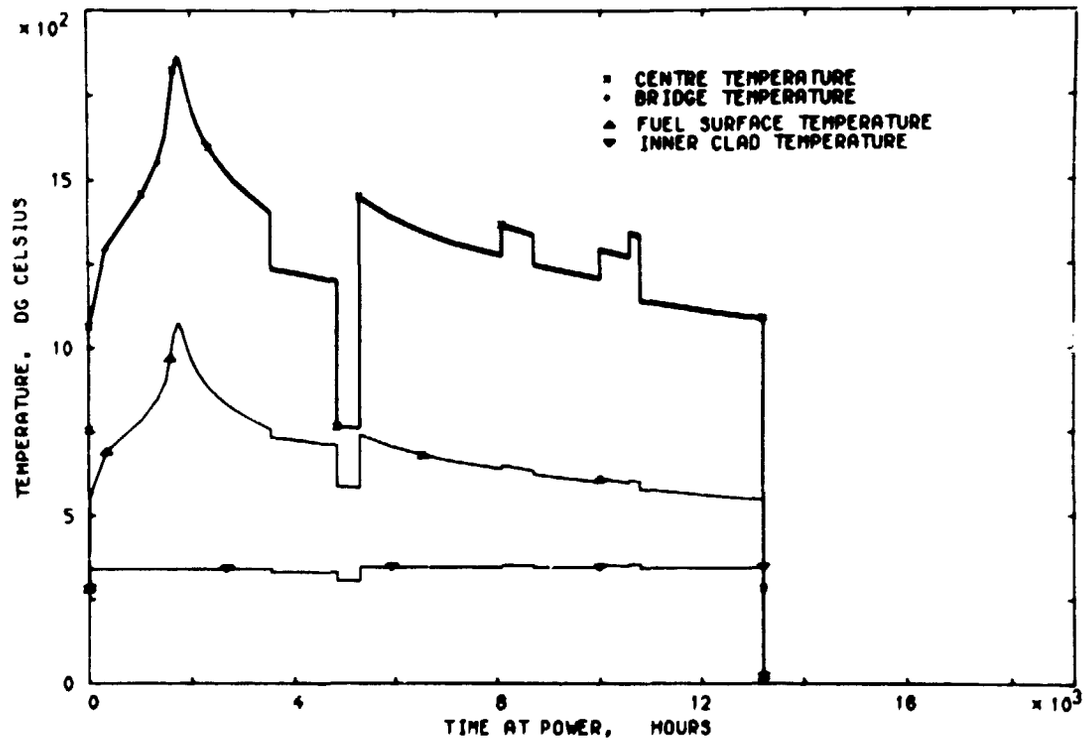

Fig. 5.6. Calculated temperatures for the PWR fuel rod.

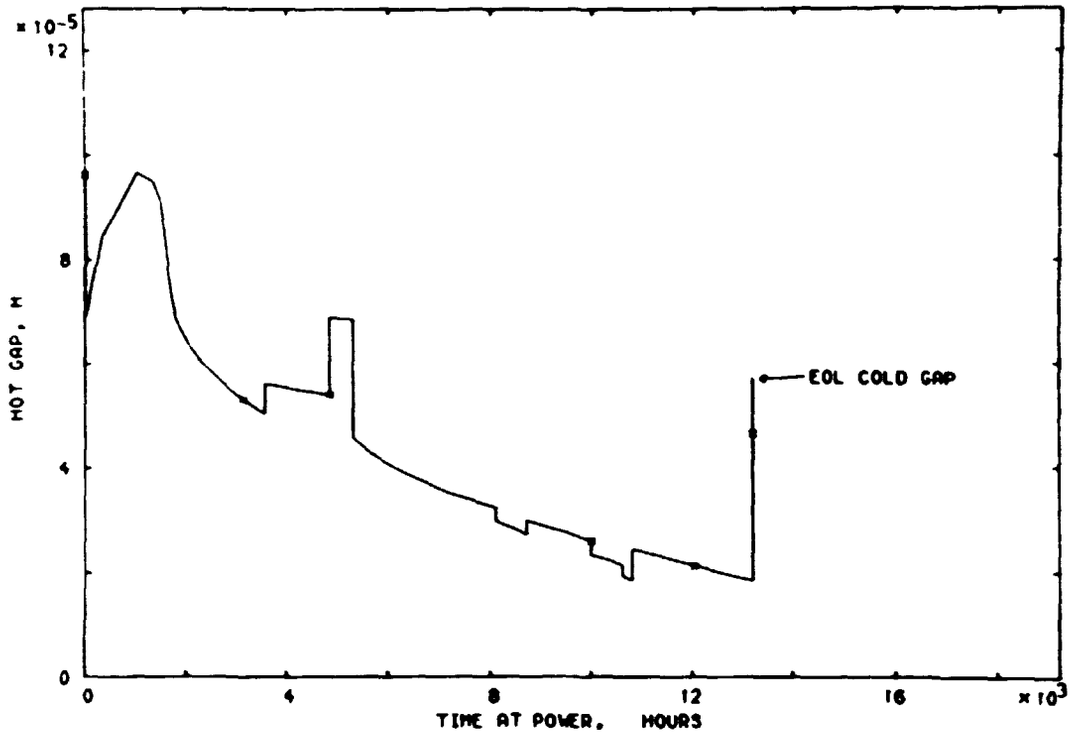

Fig. 5.7. Calculated average radial gap between fuel and cladding for the PWR fuel rod.

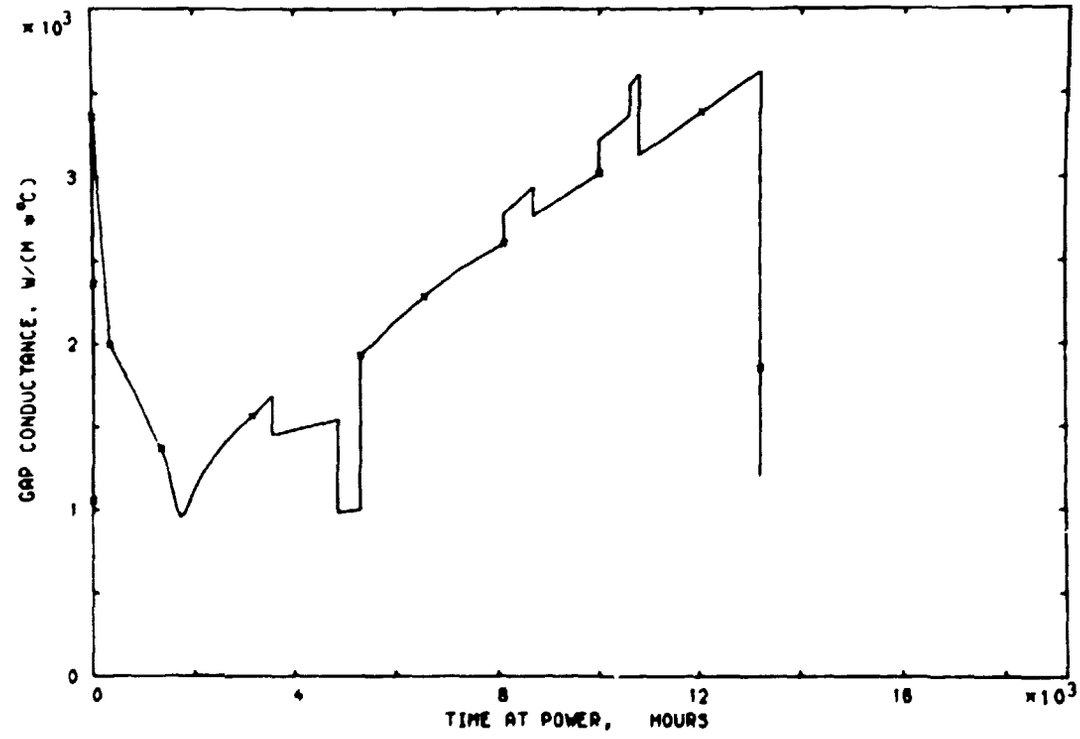

Fig. 5.8. Calculated gap conductance for the PWR fuel rod.

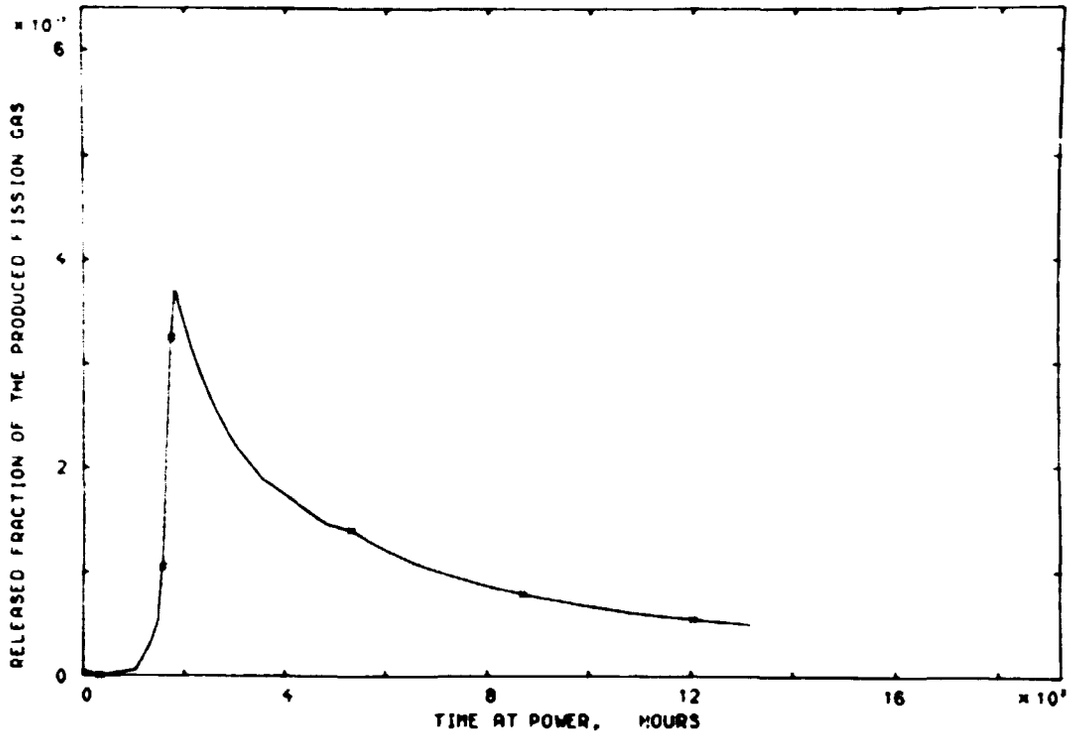

Fig. 5.9. Calculated release fraction of fission gas for the PWR fuel rod.

5.2. Verification of FFRS

The verification of a model for fuel rod simulation is very difficult. The materials differ for different fuel rods and only some of these differences are reflected in the design specifications. For the remaining material properties, some best estimate values are used.

5.2.1. Comparison with other fuel models

Since FFRS is specially developed as a fast and thus as a simple model, the physical model can well be verified through comparisons with other more detailed codes. When comparing different models with experimental data, the influence of unspecified material properties should be considered, since they can totally overshadow the physical differences in the models.

An investigation in which an attempt was made to define common best estimate values for most of the important material properties, thereby enabling a direct comparison between the

physical models, is reported in refs. 18 and 19. Comparisons between FFRS and the models included in this investigation[20] demonstrate that the physical models in FFRS can model average stresses and strains in the cladding and the temperature distribution in the fuel rod as accurately as any of these codes. The investigation did, however, indicate that the modelling of hot swelling, densification, fission gas release and perhaps gap conductance needed improvement. The only model that did not use the suggested best estimate models for hot swelling and densification (no model for gap conductance was suggested), seemed to obtain the best results in two cases with unstable fuel (large, fast densification).

5.2.2. Comparisons with irradiation experiments

The material properties used by default in FFRS were reviewed after the investigation reported in ref. 20. The models for hot swelling, densification and gap conductance in particular were improved. The set of best estimate material properties, based on data available in the open literature, is reported in ref. 3.

Comparisons between FFRS and the experimental results available from a large number of irradiation experiments are summarized in table 5.1. In the simulations the best estimate values from ref. 3 have been used for all unspecified material properties. There may be large differences in the material properties like creep, densification, yielding (especially the fluence dependence) etc., for the individual rods. Therefore one cannot expect predictions of the experimental results for each individual irradiation experiment, but the overall results from the simulations should be in good agreement with the experimental results.

The important design data are listed in table 5.2. The densification specified at 0.2% FIMA and 1.0% FIMA is the densification calculated by the model from ref. 3, where the porosity distribution in the fuel is estimated from the sintering information or from a given densification specification. Information regarding the irradiation conditions for the pins is listed in table 5.3, further information is found in the references given.

Table 5.1. Comparison between experimental data and the values calculated by means of FFRS.

	Pin no.	M20-1B	M2-2B ⟷	TY-1B	PB29-4	M2-2C	AG17-2	Ag17-3 ⟷	AG17-5	AG17-4 ⟷	AG17-6	AG17-7	HCB IPA-21	E-260	E-264	ELP-9	PWR BOP	BOP BOS	BOP & IPA-618
Experimental results	BOL average strain, %	-0.35	-0.40	-0.20	—	—	0			0	0	0	0.2-0.3	0.38	0.36	—	-0.59	—	
	Pre-ramp average strain, %	-0.40	-0.40	-0.40	—	—	-0.15 ⟷	-0.30 ⟷	-0.25	-0.17 ⟷	-0.15 ⟷	-0.12	—	—	—	—	—	—	
	Max. centre temperature, °C	1950	—	—	1300	1850	—	—	—	—	—	—	—	2015	2166	2280	1650		
	Released fission gas, %	40	33	33	47	37	3	3	3	3	1	21	6(2.3)	—	—	23-26	12.7	—	
	Temperatures, fig.no.	—	—	—	—	—	—	—	—	—	—	—	5.10,5.11	—	—	—	—		5.14
	Strain (from strain gage), fig.no.	—	—	—	—	—	—	—	—	—	—	—	—	5.12	5.13	—	—		—
Calculated values	BOL average strain, %	-0.29	-0.5	-0.5	-0.25	-0.36	-0.16	-0.17	-0.17	-0.27	-0.27	-0.22	0.16	0.21	0.16	—	-0.71	—	
	Pre-ramp average strain, %	-0.33	-0.56	-0.56			-0.17	-0.18	-0.18	-0.27	-0.27	-0.26	—	—	—	—	—	—	
	Max. centre temperature, °C	21	1800	1800	2260	2	1972	1983	1966	1700	1700	1900	—	1970	2160	2230	1860	—	
	Released fission gas, %	45	21	21	61	47	21	22	22	0	0	0	22	—	—	19	5	—	

⟷ identical in design and radiation
— not available
* failed

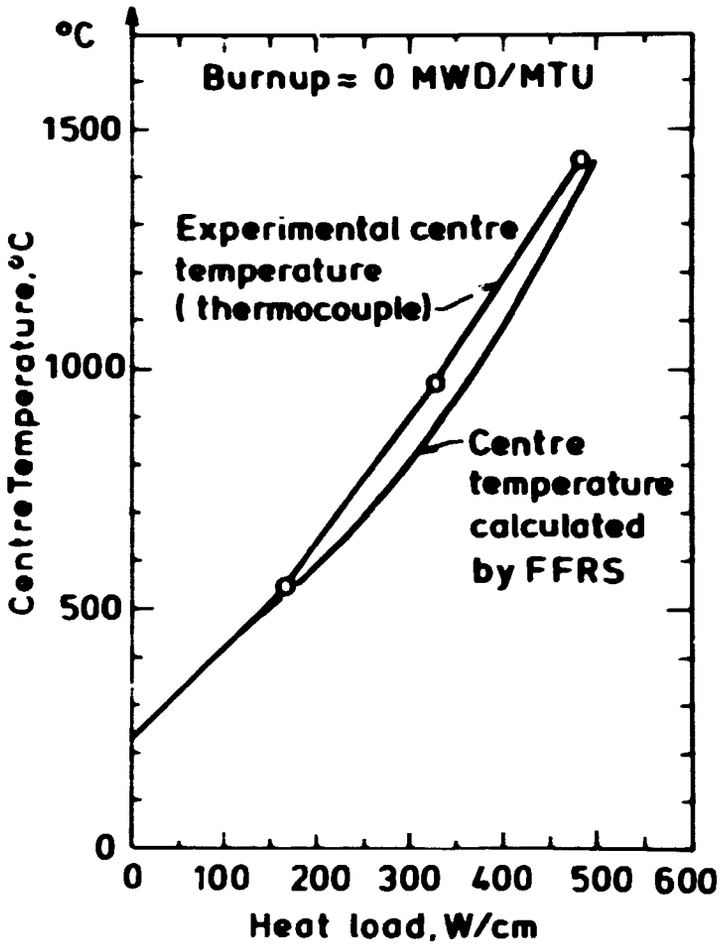

Fig. 5.10. Measured and calculated centre temperature for the HCD fuel rod at the beginning of the irradiation.

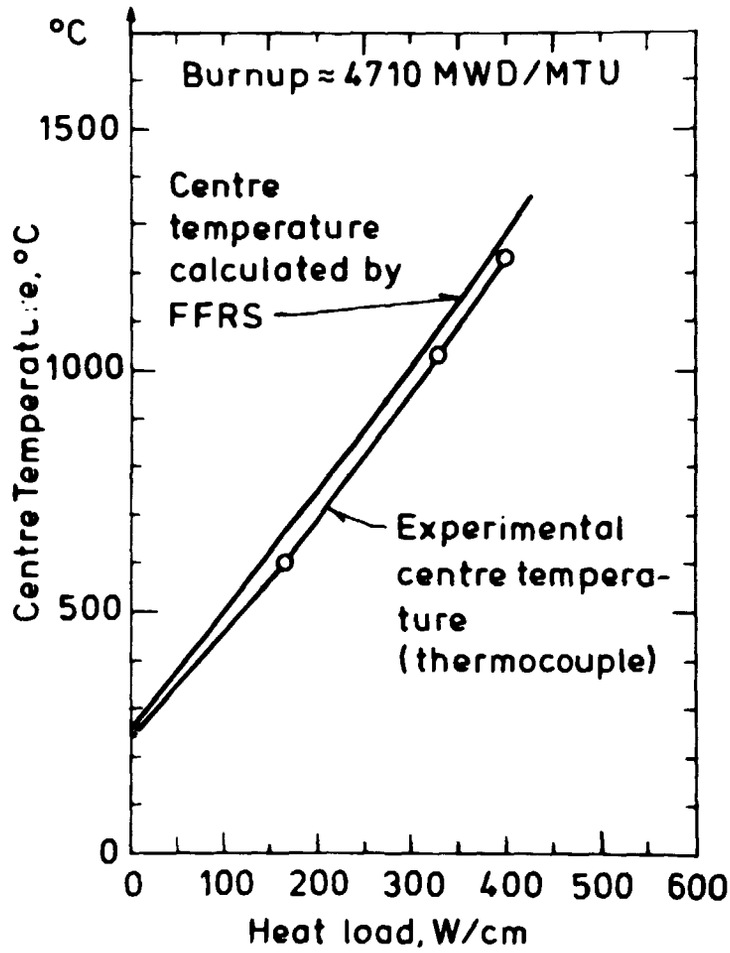

Fig. 5.11. Measured and calculated centre temperature for the HCD fuel rod at 4710 MWd/MtU.

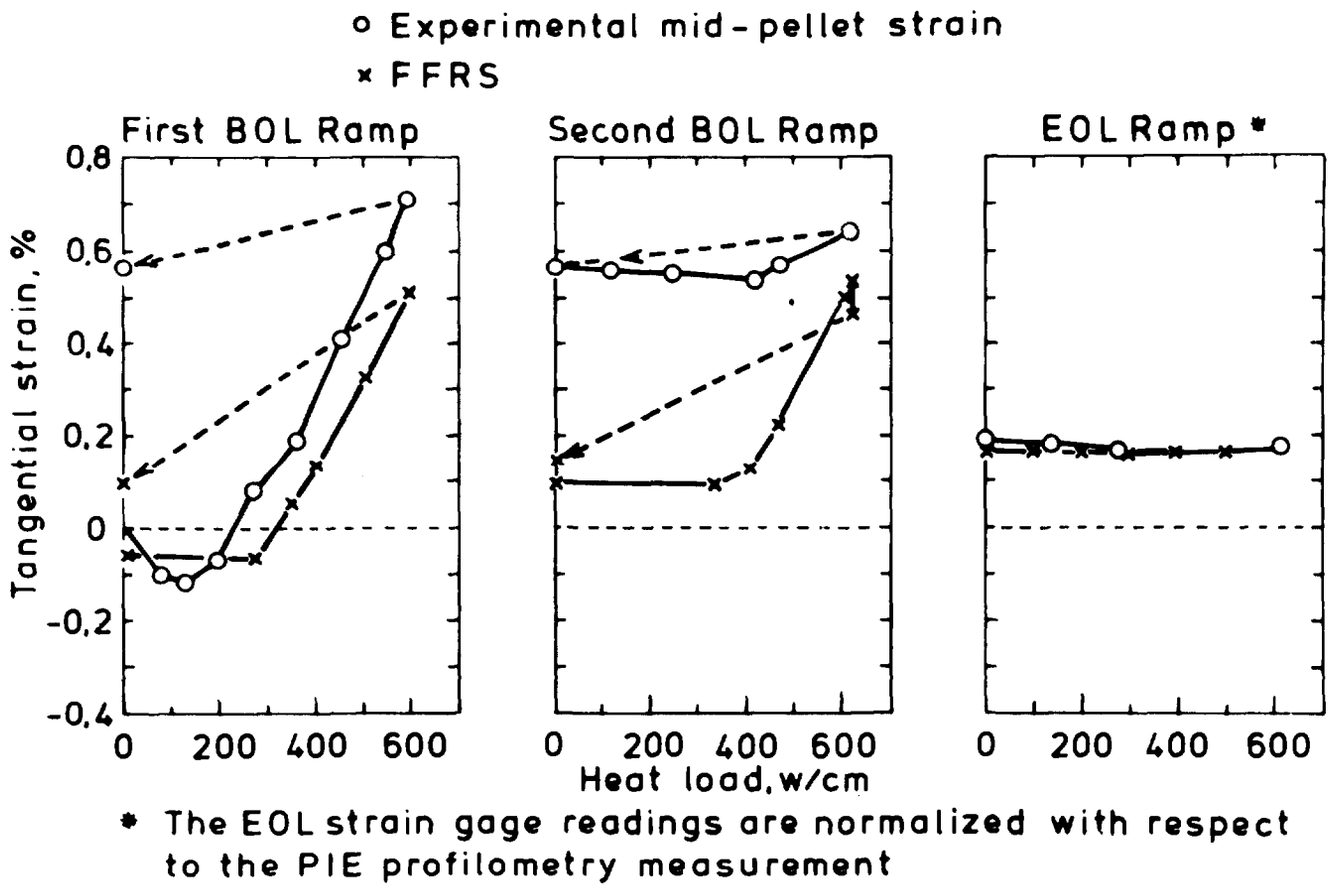

Fig. 5.12. Measured and calculated tangential strain for the X-260 fuel pin.

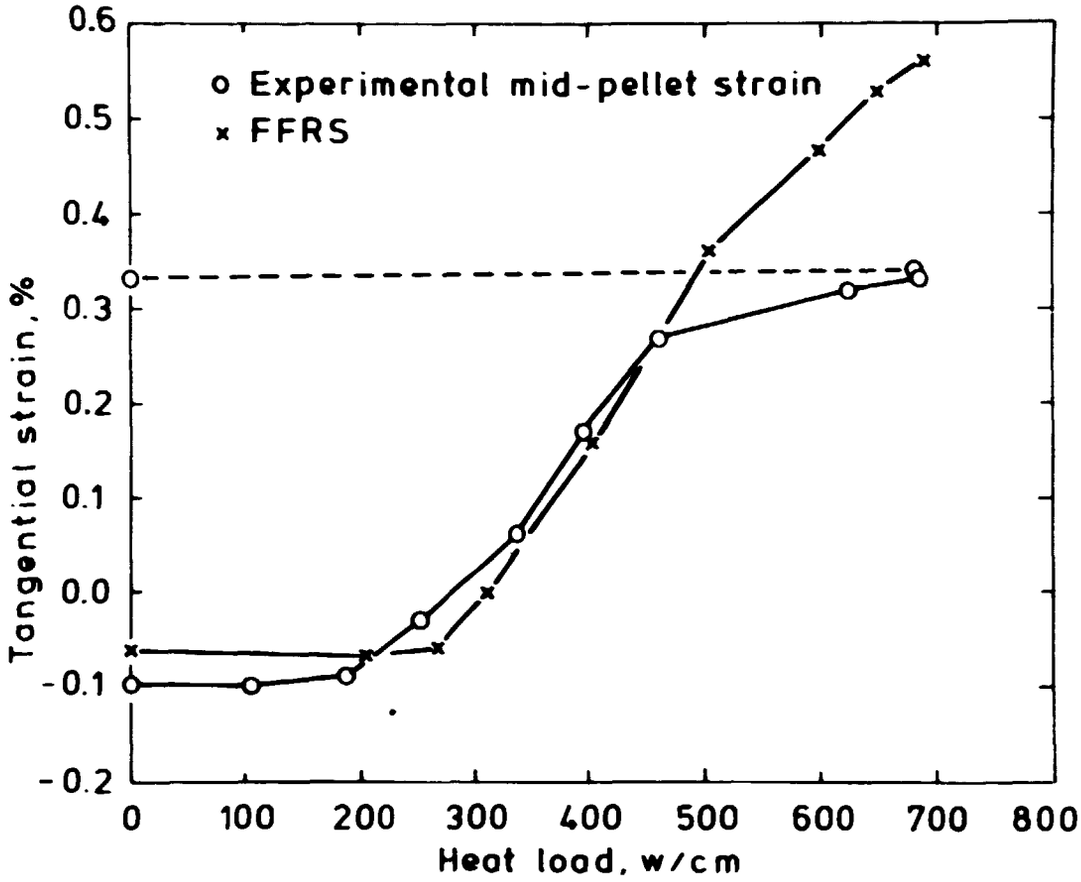

Fig. 5.13. Measured and calculated tangential strain for the X-264 fuel pin.

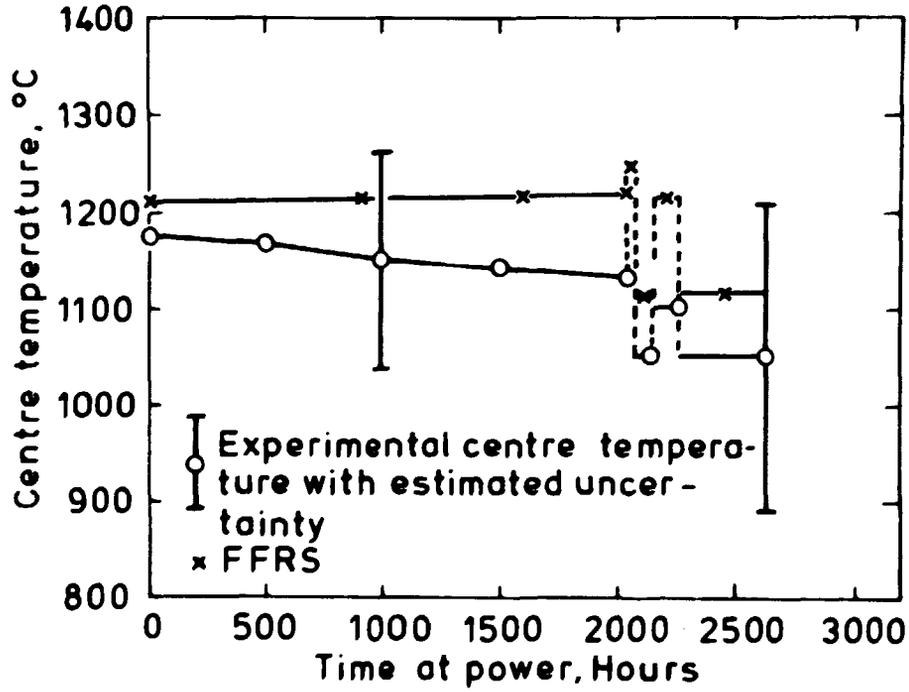

Fig. 5.14. Measured and calculated centre temperature for rod 6 in the IFA-418 experiment.

Table 5.2. Design specifications for the irradiation experiments used in the verification of FFRS.

Pin No.	M20-1B	M2-2B	T9-3S	PA29-4	M2-2C	AG17-2 AG17-3 AG17-5	AG17-4 AG17-6 AG17-7	HCD	X-260	X-264	ELP-9	PWR ROD	IFA-418 RODG
Cladding inner diameter, mm	12.84	12.85	12.87	12.84	12.84	9.68	9.48	12.6	10.7	10.7	7.57	9.86	9.30
Gap size, radial, mm	0.105	0.110	0.12	0.12	0.12	0.095	0.095	0.031	0.055	0.055	0.15	0.108	0.15
Clad thickness, mm	0.55	0.54	0.56	0.59	0.53	0.63	0.63	0.65	0.55	0.55	0.55	0.66	1.02
Stack length, m	0.125	0.126	0.127	0.128	0.128	0.129	0.129	1.71	0.48	0.38	1.0	3.67	0.75
Cold free volume, cm^3	2.80	2.8	2.8	2.9	2.9	1.27	1.27	16.	1)	1)	5.76	34	4.08
Enrichment, %	1.65	1.65	1.65	2.28	2.28	3.16	3.16	5	1.35	1.59	4.5	2.01	6.0
Fuel grain size, um	25.	25.	25.	8.	8.	20.	20.	14.	8.	8.	4.	4.	7.
Fuel density, % TD	94.4	94.4	94.4	94.7	94.7	96.	96.	95.5	97.6	96.3	94.25	93	96
Densification at 0.2% FIMA, % (assumed)	0.4	0.4	0.4	0.4	0.4	0.24	0.24	0.3	0.15	-	3.5	2.5	0.24
Densification at 1.0% FIMA, % (assumed)	1.4	1.4	1.4	1.4	1.4	1.0	1.0	1.2	0.7	-	4.5	3.5	1.0
Cladding unirr. σ_0 yield strength at 300°C, MP_a	300.	300.	305	285.	300.	430.	430	255.	290.	290.	364	364	364
Cladding roughness, um	0.9	0.9	0.9	0.9	0.9	1.0	1.0	4.0	0.51	0.51	1.0	0.25	0.25
Fuel roughness, um	1.3	1.3	1.3	0.9	0.9	0.7	0.7	1.25	1.0	1.0	3.81	2.49	2.5
Cold fill gas pressure, MP_a	0.098	0.098	0.098	0.098	0.098	2.75	2.75	0.098	1)	1)	0.33	0.098	2.21
Fill gas	He	He	He	He	He	He	He	He	He	He	He+(N_2)	He+(N_2)	He
Inverse neutron diffusion length in fuel, m^{-1}	80	80	80	125	125	150	150	175	73	85	175	130	212
Reference	17	17	17	23	23	24	25	19	19	19	19	19	18

1) Pressure kept at 1 atmosphere

The agreement between the calculated and the experimental results is very good. This is considered both as a verification of the model, FFRS, and of the best estimate material properties from ref. 3.

The largest deviations seem to be found for the temperatures in the high burn-up cases (M2-2C and PA29-4), the fission gas release for some pins (AG17-3, AG17-7 and HCD), and the interaction during the final ramp for the AG-pins.

The influence on the calculated results of changes in the assumed material properties is investigated in the following section.

Table 5.3. Irradiation conditions for the irradiation experiments used in the verification of FFRS.

Pin no.	M20-1B	M2-2B T9-3B	PA29-4 M2-2C	AG17-2	AG17-3 AG17-5	AG17-4 AG17-6	AG17-7	HCD IFA-21	X-260	X-264	ELP-9	PWR JBP 005	BOD6 IFA-418
Irradiation facility[a]	DR3	DR3	DR3	DR3	DR3	DR3	DR3	HBWR	NRX	NRX	ELP3	CE-PWR	HBWR
Coolant pressure, MP_a	6.9	6.9	6.9	14.8	14.8	14.8	14.8	2.9	8.0	8.0	0.34	12.4	2.9
Cladding surface temperature, °C	293	293	293	340	340	340	340	245	251	251	115	325	245
Fast neutron flux at max. power, n/cm^2-sec	3×10^{13}	3×10^{13}	3×10^{13}	3×10^{13}	3×10^{13}	3×10^{13}	3×10^{13}	3×10^{13}	1×10^{13}	1×10^{13}	1×10^{12}	7.5×10^{13}	3×10^{13}
EOL burnup, MWd/tUO_2	27600	30000	38000-40000	11200	11200	17100	18800	10600	1500	~0	15000	11800	—
Pre ramp heat load, W/cm	280-570	280-570	370-590	340-510	340-510	295-470	295-470	384-480	660	—	390-610	85-270	—
Heat load just before ramp, W/cm	360	280	—	340	340	295	295	400	660	—	—	—	—
Max. ramp heat load, W/cm	480	480	—	540	540	495	435-455	512	615	—	—	—	—
Ramp rate, W/cm-hour	1600	1550	—	12000	12000	750	1200	65	260	260	—	—	—

[a] DR3 = Danish testreactor, HBWR = Halden Boiling Heavy Water Reactor in Norway
NRX = Canadian testreactor, ELP3 = Experimental Heavy Water Reactor in France

5.3. Sensitivity studies

For eight of the pins investigated, the results of calculations with different assumptions regarding some of the unspecified material properties are listed in tables 5.4-5.10. The material properties are only varied to values that are very likely to occur. Often the values used in these calculations are just as reasonable as those used for the Base Calculations shown in table 5.1.

5.3.1. Fission gas release

In table 5.4 the results from calculations with 2 additional fission gas release models are shown. The model used in the Base Calculations is that proposed by Lewis[21]. The BNWHT model is that used for the calculations reported in ref. 19. LOOPY[22] is a Swedish model. There is no reason for choosing any one specific model. However, as seen in table 5.4, the results,

Table 5.4. Results from simulations with different fission gas release models.

	Pin no.	M20-1B	PA29-4	AG17-3 AG17-5	AG17-4 AG17-6	BCD	S-260	ELP-9	PWR ROD JBP 005
PIE DATA	EOL average strain, %	-0.35	—	-0.17-0.0	-0.1-0.0	0.2-0.3	0.28	—	-0.59
	Max. centre temperature, °C	1950	1900	—	—	1232*	2015	2200	1650
	Released fission gas, %	40	47	3	9	2.3%	—	23-26	12.7
BASE CALC. Lewis release model	EOL average strain, %	-0.29	-0.25	-0.17	-0.27	0.16	0.21	—	-0.71
	Max. centre temperature, °C	2100	2260	1960	1700	1268	1970	2230	1860
	Released fission gas, %	35	61	22	8	22	—	19	5
BNWHT's release model	EOL average strain, %	-0.28	-0.23	-0.17	-0.27	0.16	—	—	-0.72
	Max. centre temperature, °C	2040	2250	1960	1700	1215	—	2230	1640
	Released fission gas, %	17	45	14	3	12	—	14	1
Loopy release model	EOL average strain, %	-0.29	-0.29	-0.17	-0.27	-0.17	—	—	-0.72
	Max. centre temperature, °C	2070	2260	1960	1700	1500	—	2210	1850
	Released fission gas, %	28	50	18	6.9	18	—	15.6	4

* at 4710 MWd/MTu and 600 W/cm

calculated with the model proposed by Lewis, generally show the best agreement with the experiments.

It should be noted that the calculated maximum temperature for the M20-1B pin occurs shortly after the beginning of the irradiation.

The small observed fission gas release for AG17-3 and the HCD rod may be explained by the fact that both rods were only kept at overpower for a short time in the end-of-life ramp test, as there were failed rods in the assemblies. All the release models used only predict the stationary release.

5.3.2. Gap conductance

The differences between the calculated and the experimental temperatures are probably caused by deviations between the calculated and the actual gap conductance.

The contact conductance, calculated by the Ross and Stoute[13] equation, and the open gap conductance calculated with the modifications proposed by Kjærheim and Rolstad[11], or Vitanza[12], have been verified on a large number of irradiation experiments equipped with thermocouples in the Halden reactor[11,12]. Unfortunately, all the experiments have approximately the same surface roughnesses (an important parameter in the Ross and Stoute expression for contact conductance), and none of the thermocouples lasted more than approximately 5000 MWd/tUO_2. For fuel rods with a high content of fission gas (high burn-up), the Ross and Stoute model predicts a low gap conductance even during contact between fuel and cladding. This has not yet been verified experimentally (at high burn-up) and it seems in conflict with the high burn-up pins (PA29-4 and M2-2C). The model used for gap conductance therefore had a lower limit for the contact conductance (in the Base Calculation equal to one third of the initial value of the gap conductance).

The influence of the assumption regarding excentricity is shown in table 5.5. As expected, the effect on the low gap cases is negligible, and even on the high gap cases the effect is moderate. This is due to hot swelling, which closes the gap at an earlier stage (before the maximum power for the ELP-9 and the PWR rod).

Table 5.5. Influence of the assumed excentricity.

Pin No.	M20-1B	PA29-4	AG17-3 AG17-5	AG17-4 AG17-6	BCD	X-260	ELP-9	PWR ROD JBP 005
EOL average strain, %	-0.35	—	-0.17-0.0	-0.1-0.0	0.2-0.3	0.28	—	-0.59
Max. centre temperature, °C	1950	1900	—	—	1212*	2015	2200	1650
Released fission gas, %	60	47	3	0	2.3%	—	23-26	12.7
EOL average strain, %	-0.29	-0.25	-0.17	-0.27	0.16	0.21	—	-0.71
Max. centre temperature, °C	2130	2260	1960	1700	1268	1970	2230	1860
Released fission gas, %	35	61	22	0	22	—	19	5
EOL average strain, %	-0.29	-0.26	-0.18	-0.27	0.16	0.21	—	-0.72
Max. centre temperature, °C	2130	2260	1970	1620	1250	1970	2250	1700
Released fission gas, %	36	61	23	0.5	22	—	19	2.4
EOL average strain, %	-0.28	-0.26	-0.15	-0.26	0.16	0.21	—	-0.61
Max. centre temperature, °C	2100	2260	2300	2170	1281	1970	2230	2370
Released fission gas, %	36	61	22	0	22	—	19	12.8

* at 4*10 MWd/MTU and 400 W/cm

Table 5.6. Influence of the contact gap conductance.

Pin No.	M20-1B	PA29-4	AG17-3 AG17-5	AG17-4 AG17-6	BCD	X-260	ELP-9	PWR ROD JBP 005
EOL average strain, %	-0.35	—	-0.17-0.0	-0.1-0.0	0.2-0.3	0.28	—	-0.59
Max. centre temperature, °C	1950	1900	—	—	1232*	2015	2200	1650
Released fission gas, %	60	47	3	0	2.3%	—	23-26	12.7
EOL average strain, %	-0.29	-0.25	-0.17	-0.27	0.16	0.21	—	-0.71
Max. centre temperature, °C	2100	2260	1960	1700	1268	1970	2230	1860
Released fission gas, %	35	61	22	0	22	—	19	5
EOL average strain, %	-0.32	-0.33	-0.17	-0.27	0.16	0.21	—	-0.71
Max. centre temperature, °C	1970	2030	1960	1700	1202	1970	1820	1740
Released fission gas, %	20	50	22	0	6	—	5	3
EOL average strain, %	-0.28	-0.21	-0.17	-0.27	0.16	0.21	—	-0.71
Max. centre temperature, °C	2130	2160	1960	1700	1268	1970	2520	1860
Released fission gas, %	42	66	22	0	35	—	38	5

* at 4*10 MWd/MTU and 400 W/cm

Table 5.6 shows the different assumptions for the minimum gap conductance during contact. As expected, these assumptions have much influence on the maximum temperatures and gas releases calculated. However, it should be noted that even the assumed unchanged gap conductivity is insufficient, in the high burn-up case, PA29-4, to explain the low center temperature.

5.3.3. Creep in fuel and cladding

Table 5.7 shows the influence of different assumptions concerning the cladding texture and the fuel and cladding creep rate.

Table 5.7. Influence of the zircaloy and UO_2 creep.

Pin no.	R20-1B	PA29-4	AG17-1 AG17-5	AG17-6 AG17-6	WC8	R-260	ELP-9	PWR 900 JBW 005
EOL average strain, %	-0.35	—	-0.17-0.0	-0.1-0.0	0.2-0.3	0.28	—	-0.59
Max. centre temperature, °C	1950	1900	—	—	1232*	2015	2200	1650
Released fission gas, %	40	47	3	5	2.39	—	23-26	12.7
EOL average strain, %	-0.29	-0.25	-0.17	-0.27	0.16	0.21	—	-0.71
Max. centre temperature, °C	2100	2260	1960	1700	1268	1970	2230	1860
Released fission gas, %	35	61	22	8	22	—	19	5
EOL average strain, %	-0.38	-0.33	-0.26	-0.41	0.19	0.21	—	-1.07
Max. centre temperature, °C	2100	2250	1960	1700	1270	1970	2230	1790
Released fission gas, %	35	61	22	8	21	—	19	6
EOL average strain, %	-0.35	-0.32	-0.21	-0.33	0.16	0.20	—	-0.85
Max. centre temperature, °C	2100	2260	1960	1700	1277	1980	2230	1860
Released fission gas, %	37	61	22	8	24	—	19	5

* at 4710 MWd/MTU and 400 W/cm

In the Base Calculations the cladding was assumed to be anisotropic with the anisotropy factors from ref. 19. The eight cases have been recalculated, assuming isotropic cladding.

All the creep equations given in ref. 3 have the uncertainty included in a single log-normally distributed stochastic variable (F_{Zr} and F_{UO_2}). The Base Calculations were performed with $F_{Zr} = 1.0$ and $F_{UO_2} = 0.5$, corresponding to the mode of the distributions. An additional simulation with $F_{Zr} = 1.2$ and

F_{UO_2} = 1.7, corresponding to the average values, is included in table 5.7.

The agreement between the calculated average EOL strain and the experimental EOL strain is excellent, the deviations are of the same size as typical differences observed for nominally equal (in design and irradiation) pins. The Base Calculations are in most of the cases closest to the experimental strains, but the deviations are only significant for the PWR rod with assumed isotropy.

5.3.4. Hot swelling and densification

The models for hot swelling and densification are based on very few experimental results. The best estimate values used could easily have been chosen a factor of two (or more) larger or smaller. The influence of a variation of a factor of two on hot swelling and densification is illustrated in tables 5.8 and 5.9.

The densification rate is of little influence in the simulations, the influence is only significant for the PWR rod.

Table 5.8. Influence of hot-swelling.

* at 6%, end of ana. 631 W/cm

As seen in table 5.8, different assumptions regarding the hot swell rate can quite strongly influence the results from the simulations.

Table 5.9. Influence of densification.

	Pin No.	M20-1B	PA29-4	AG17-3 AG17-5	AG17-4 AG17-6	HCD	X-260	ELP-5	PWR ROD JBP 005
PIE DATA	EOL average strain, %	-0.35	—	-0.17-0.0	-0.1-0.0	0.2-0.3	0.28	—	-0.59
	Max. centre temperature, °C	1950	1900	—	—	1232*	2015	2200	1650
	Released fission gas, %	40	47	3	5	2.3	—	23-26	12.7
BASE CASE	EOL average strain, %	-0.25	-0.25	-0.17	-0.27	0.16	0.21	—	-0.71
	Max. centre temperature, °C	2100	2260	1960	1700	1268	1970	2230	1860
	Released fission gas, %	35	61	22	8	22	—	19	5
Densification rate = half of base value	EOL average strain, %	-0.29	-0.22	-0.18	-0.27	0.14	0.20	—	-0.71
	Max. centre temperature, °C	2100	2260	1970	1700	1271	1980	2230	1930
	Released fission gas, %	36	61	23	10	28	—	21	5
Densification rate = double of base value	EOL average strain, %	-0.23	-0.23	-0.17	-0.27	0.21	0.21	—	-0.72
	Max. centre temperature, °C	2090	2250	1960	1700	1257	1970	2230	1870
	Released fission gas, %	34	61	22	8	19	—	19	4

* at 4710 MWd/MTU and 400 W/cm

5.3.5. Helium content in the rods

In the design specification for the two unstable fuel rods (ELP-9 and the PWR rod), the as-fabricated cold gas pressure was 1 atm, but the content of He found in the rods during the PIE*) was considerably higher, namely corresponding to approximately 3 atm He pressure in the ELP-9 rod and approximately 2 atm in the PWR rod. This additional content of helium may be explained by ternary fission and/or rest gas from fabrication. A calculation in which this additional gas is assumed present from the beginning of irradiation is shown in table 5.10.

The influence of this additional gas is very strong, but it is difficult to know exactly when the release of the helium takes place.

*) Post Irradiation Examination

Table 5.10. Influence of helium content in the fuel.

	Pin no.	ELP-9	PWR ROD JB 005
PIE DATA	EOL average strain, %	—	-0.59
	Max. centre temp., °C	2200	1650
	Released fission gas, %	23-26	12.7
Base calculations	EOL average strain, %	—	-0.71
	Max. centre temperature, °C	2230	1850
	Released fission gas, %	19	5
	Cold helium, pressure, atm.	1	1
Additional helium	EOL average strain, %	—	-0.71
	Max. centre temperature, °C	1930	1580
	Released fission gas, %	7	2
	Cold helium pressure, atm.	3	2

5.4. Calculation times

The computer code FFRS is written in Fortran IV and implemented on the B6700**) installation at Risø. The calculation times for the eight examples used in the sensitivity studies are shown in table 5.10. The code is also implemented on the CDC 6600***) installation in Stockholm. Calculation of the M20-1B case gave a factor of 7 between the calculation times using the two computers (the factor is typically 10 for other codes). Based on this factor, the calculation times were estimated for the eight cases using the CDC 6600 computer.

Table 5.11. Calculation times.

Pin no.	M20-1B	PA29-4	AG17-3 AG17-5	AG17-4 AG17-5	HCD	X-260	ELP-9	PWR
CPU time on B6700 in seconds	13	30	7	7	8	12	17	7
Estimated CPU time on CDC6600 in seconds	1.9	4.3	1.0	1.0	1.1	1.7	2.4	1

**) Burroughs Computer

***) Control Data Cooperation

6. CONCLUSION

The fuel model FFRS is presented. It is shown that, in spite of its simplicity, FFRS very accurately models average pellet-cladding interaction. Comparison with other fuel models show that the accuracy obtained in calculations with FFRS are comparable to that obtained by typical state-of-the-art fuel models, although the calculation times are two to three orders of magnitude shorter.

The model has been verified together with the material data used, through the simulation of a large number of irradiation experiments. Together with sensitivity studies, these simulations show that the deviations between the results calculated by FFRS and the experimental results can easily be explained by differences in unspecified material properties. The only significant deviation is the temperature prediction for the high burn-up cases. This must be ascribed to deviations in the calculated and the actual contact conductivity between zircaloy and UO_2.

REFERENCES

1. Kjær-Pedersen, N. (1977). A New Version of the LWR Fuel Performance Model WAFER. In: Transactions of the 4. International Conference on Structural Mechanics in Reactor Technology, San Francisco, Calif., 15-19 August 1977. Edited by T.A. Jaeger and B.A. Boley. Vol. D. (Commision of the European Communities, Luxembourg). Paper no. D13.

2. ODQVIST, F.K.G. (1966). Hållfasthetslära. 3.th.rev.ed. (Natur och Kultur, Stockholm) 815 pp.

3. Misfeldt, I. (1978). Material Properties for LWR Fuel Rod Modelling. Risø National Laboratory, Risø-M-2117.

4. Hill, R. (1960). The Mathematical Theory of Plasticity (University Press, Oxford) 355 pp.

5. El-Wakil, M.M. (1962). Nuclear Power Engineering (McGraw-Hill, New York) 556 pp.

6. Stehle, H. and Assmann, H. (1974). The Dependence of In-Reactor UO_2 Densification on Temperature and Microstructure. J. Nucl. Mater. 52, 303-308.

7. Notley, M.J.F., Bain, A.S., and Robertson, J.A.L. (1964). The Longitudial and Diametral Expansion of UO_2 Fuel Elements. Atomic Energy of Canada Ltd., AECL-2143, 14 pp.

8. Wordsworth, J. (1974). IAMBUS-1, - A Digital Computer Code for the Design, In-Pile Performance Prediction and Post-Irradiation Analysis of Arbitrary Fuel Rods. Part 1: Theory and modelling. Nucl. Eng. Des. 31, 309-336.

9. Howl, D. Private Communication.

10. Meyer, R.O. Private Communication.

11. Kjærheim, K. and Rolstad, E. (1967). In-Pile Determination of UO_2 Thermal Conductivity, Density Effects and Gap Conductance. Institutt for Atomenergi. Halden Reactor Project, HPR-80, 85 pp.

12. Vitanza, C. Private Communication.

13. Ross, A.M. and Stoute, R.L. (1962). Heat Transfer Coefficient between UO_2 and Zircaloy-2. Atomic Energy of Canada Ltd., AECL-1552, 67 pp.

14. Gittus, J.H., Howl, D.A., and Hughes, H. (1970). Theoretical Analysis of Cladding Stresses and Strains Produced by Expansion of Cracket Fuel Pellets. Nucl. Appl. Technol. 9, 40-46.

15. See ref. no. 7.

16. Hann, C.R., Beyer, C.E., and Parchen, L.J. (1973). Gapcon Thermal-1: A Computer Program for Calculating the Gap Conductance in Oxide Fuel Pins. Battelle-Northwest. Pacific Northwest Lab., BNWL-1778, 235 pp.

17. Knudsen, P. (1977). Ramp Testing of UO_2-ZR Fuel Pins up to 29,000 MWD/MT UO_2. Trans. Am. Nucl. Soc. 27, 244-245.

18. Freeburn, H.R., Pati, S.R., and Fiero, I.B. (1977). Light Water Reactor Fuel Rod Modeling Code Evaluation. Final Report. Electric Power Research Institute, EPRI-NP-369. 267 pp.

19. Andrews, M.G., Freeburn, H.R., and Pati, S.R. (1976). Light Water Reactor Fuel Rod Modeling Code Evaluation, Phase II Topical Report. Combustion Engineering Inc. Nuclear Power Department. CENPD-218. Various pag.

20. Misfeldt, I. (1977). Performance of the Fuel Model FFRS. Risø National Laboratory, Risø-M-1928, 11 pp.

21. Lewis, W.B. (1966). Engineering for the Fission Gas in UO_2 Fuel. Nucl. Appl. 2, 171-181.

22. Joon, K. Private Communication.

23. Knudsen, P. and Carlsen, H. Private Communication.

24. Knudsen, P., Bagger, C., and Fishler, M. (1977). Characterization of PWR Power Ramp Tests. In: ANS Topical Meeting on Water Reactor Fuel Performance, 9-11 May 1977, St.Charles, Ill., May 9-11, 1977 (American Nuclear Society, LaGrange Park, Ill.) 243-252.

25. Knudsen, P. Private Communication.

ISBN 87-550-0510-1
ISSN 0418-6443